UNDERWATER APPLICATIONS OF ACOUSTO-OPTICAL IMAGING

R. A. Smith, et al

TRW Systems Group

Prepared for:

Office of Naval Research
Defense Advanced Research Projects Agency

29 March 1974

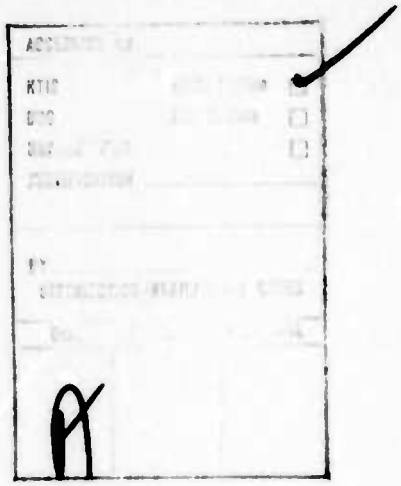

Principal Investigator: R. A. Smith, TRW Systems Group
(213) 536-1845

ONR Scientific Officer: R. F. Obrochta

Contract Amount: $179,000

Contract Period: 1 January 1972 - 29 March 1974

Unclassified

SECURITY CLASSIFICATION OF THIS PAGE (When Data Entered)

REPORT DOCUMENTATION PAGE

READ INSTRUCTIONS BEFORE COMPLETING FORM

1 REPORT NUMBER

2 GOVT ACCESSION NO.

3 RECIPIENT'S CATALOG NUMBER
AD-784 419

4 TITLE (and Subtitle)
Underwater Applications of Acousto-Optical Imaging

5 TYPE OF REPORT & PERIOD COVERED
Final Report

6 PERFORMING ORG. REPORT NUMBER
AT-SVD-TR-74-7

7 AUTHOR(s)
R. A. Smith and J. H. Cole

8 CONTRACT OR GRANT NUMBER(s)
N00014-72-C-0182

9 PERFORMING ORGANIZATION NAME AND ADDRESS
TRW Systems Group
One Space Park
Redondo Beach, California 90278

10 PROGRAM ELEMENT, PROJECT, TASK AREA & WORK UNIT NUMBERS
Code 411
Purchase REquest NR 240-030

11 CONTROLLING OFFICE NAME AND ADDRESS
Tactical Technology Off., Attn. Cdr. J. Seesholtz
Defense Advanced Research Projects Office
Arlington, Virginia 22209

12 REPORT DATE
29 March 1974

13 NUMBER OF PAGES
71

14 MONITORING AGENCY NAME & ADDRESS (if different from Controlling Office)
Office of Naval Research
Arlington, Virginia

15 SECURITY CLASS. (of this report)
Unclassified

15a DECLASSIFICATION/DOWNGRADING SCHEDULE

16 DISTRIBUTION STATEMENT (of this Report)
Approved for public release; distribution unlimited.

17 DISTRIBUTION STATEMENT (of the abstract entered in Block 20, if different from Report)

18 SUPPLEMENTARY NOTES
Robert F. Obrochta
ONR Scientific Officer
(202) 692-4413

19 KEY WORDS (Continue on reverse side if necessary and identify by block number)
Imaging Sonar
Ocean Surveillance
Bragg Imaging
Underwater Inspection System
Raman-Nath Imaging

20 ABSTRACT (Continue on reverse side if necessary and identify by block number)
The results of experiments and analyses completed during Phase 2 concerning the performance of the TRW acousto-optical imaging system are presented. The ultimate sensitivity of the system is reviewed from a theoretical viewpoint and it is shown that the theoretical limit for the system is an echo intensity of about -60 dB relative to a μbar. Experiments were carried out substantiating theoretical predictions. Thus system sensitivity is considerably better than earlier believed. Laboratory experiments on resolution and field

DD FORM 1 JAN 73 1473 EDITION OF 1 NOV 65 IS OBSOLETE

Unclassified

SECURITY CLASSIFICATION OF THIS PAGE (When Data Entered)

of view were carried out with an acoustic reflector in place. Resolution somewhat better than twice the theoretical limit was observed. It is shown that an acoustic reflector can be used to form a field of view as large as 100 degrees. Experiments are reported describing the performance of the Bragg cell at lowered water temperatures. Best performance was obtained at about 4°C.

TRW
SYSTEMS GROUP

UNDERWATER APPLICATIONS OF ACOUSTO-OPTICAL IMAGING

FINAL REPORT

AT-SVD-TR-74-7

29 March 1974

R. A. Smith and J. H. Cole
Advanced Technology Staff
Space Vehicles Division

Sponsored by

Defense Advanced Research Projects Agency
Arlington, Virginia 22209

ARPA Order No. 1951, Program Code No. 3N10

Prepared for

Office of Naval Research
Arlington, Virginia

Contract No. N00014-72-C-0182
Contract Authority NR 240-030

TRW SYSTEMS GROUP
One Space Park
Redondo Beach, California 90278

TRW SYSTEMS GROUP

FOREWORD

This report was prepared by the Advanced Technology Staff, Space Vehicles Division, TRW Systems Group, Redondo Beach, California, under contract N00014-72-C-0182 with the Office of Naval Research, Arlington, Virginia. The project was sponsored by the Defense Advanced Research Projects Agency under ARPA Order number 1951. The authors wish to thank Commander John R. Seesholtz of ARPA and Mr. Robert Obrochta, Code 411, Vehicle and Warfare Technology, Naval Applications Analysis Division, ONR, for the valuable technical discussions and the guidance provided during the course of this investigation. The authors also wish to acknowledge the assistance provided by Cliff Murrow in performing the laboratory experiments. The work was performed in the Advanced Technology Staff of Space Vehicles Division which is under the direction of Drs. R. L. Johnson and P. G. Bhuta.

TRW
SYSTEMS GROUP

TABLE OF CONTENTS

		Page
1.0	SUMMARY	1
2.0	REVIEW OF BASIC WORKING PRINCIPLES	7
2.1	Imaging Principles	7
2.2	Sensitivity	9
2.2.1	Light Diffracted by the Sound Signal	12
2.2.2	Brillouin Scatter	20
2.2.3	Signal Intensity for Fifty Percent Contrast in the Orthoscopic Plane	22
2.2.4	Image Pickup by Optical Heterodyning	25
3.0	PROJECTED RANGE PERFORMANCE SONAR	29
3.1	Sensitivity Experiments	29
3.2	Range Calculations	30
4.0	LABORATORY EXPERIMENTS	41
4.1	Resolution	41
4.2	Resolution with a Parabolic Reflector	43
4.2.1	Field of View	46
4.3	Range Azimuth Imaging	48
4.4	Improvement of Image Quality	52
4.4.1	Turbulent Mixing in the Light/Sound Interaction Region	53
4.4.2	Cooling of the Light/Sound Interaction Region to 4°C	55
4.5	Dual Frequency Heterodyning	55
5.0	CONCLUSIONS	62
6.0	REFERENCES	63

TRW SYSTEMS GROUP

1.0 SUMMARY

Under ARPA order No. 1959, TRW Systems is investigating acousto-optical imaging techniques for various sonar applications. The results of an earlier phase of this investigation were reported in Reference 1. This work included the demonstration of the formation of acousto-optical images in the frequency range of interest for sonar applications and, in general, completed a preliminary assessment of the imaging performance of the Bragg cell. Under the second phase of the project which is covered by this report, an up-graded system was designed utilizing light heterodyning to form the images and a more extensive examination, both analytical and experimental, of the potential performance of the acousto-optical imaging system was carried out. In addition, during the fall of 1973, it became apparent to both government and TRW personnel that some aspects of the acousto-optical imaging technique might have advantages over conventional sonar when used for the inspection of the interior of optically opaque undersea objects. Accordingly, in November 1973, emphasis, judged to be within the scope of the current contract, was placed upon these applications at the direction of cognizant DoD personnel. This report also contains progress to date on those tasks.

Significant progress in the development of the acousto-optical imaging technique for underwater imaging was made during the current period. Highlights of the progress are summarized in the paragraphs below.

1. As is the case with all imaging systems, noise determines the ultimate limit of the acousto-optical system sensitivity. The source of noise in the acousto-optical Bragg cell are (1) Brillouin scattering or scattering of the laser due to thermal phonons and (2) extraneous scattered light, the source of which is imperfections in the optics or the presence in the Bragg cell of small particles of extraneous matter. Careful investigation of these effects was carried out leading to the conclusion that the theoretical limit of the sensitivity of the acousto-optical imaging system is lower than that previously reported in Reference 1. The estimated theoretical sensitivity corresponds to detection of signal sound of about - 100 dB. This prediction was generally verified by improved measurements of the sensitivity threshold.

Measurement down to a sound pressure level of -20.6 dB (relative to 1 μbar) was completed. This is an improvement of 34.3 dB over those values previously reported in Reference 1. Details of the sensitivity analysis may be found in Section 2.2. Experimental results are summarized in Section 3.1.

2. Estimated range and resolution performance of the system was calculated and reported in Reference 1. These calculations were based on a threshold determined experimentally by using a conservative estimate that all power into the observed transducer was converted to sound. An NRL calibrated transducer was recently obtained and used which showed 30 dB greater sensitivity was correct. As a result range calculations were revised. Detailed performance predictions are contained in Section 3.2.

3. Experiments were performed with the Bragg cell cooled to remove the distorting effects of thermal gradients. Best results are obtained with the water temperature at about 4°C. Operational advantage can be realized from this feature of the imaging system in applications for object inspection at large depths.

Since the acousto-optical imaging system is not a conventional sonar system, a brief description of its principles of operation and its performance characteristics are included here for convenience.

The acousto-optical system under investigation transfers the acoustical image formed by reflected sound waves to light diffracted from a laser beam in water receiving reflected sound. The configuration considered is in the form of the Bragg imaging system[3-7]. This system operates with an expanded beam of laser light which is brought to a line of focus just beyond the water filled region receiving sound reflected from the object viewed. Anamorphic images are formed in the side bands of light (either side of cell illumination) due to interaction of sound in the water filled volume which also receives both light and sound. A good image of an object in media, opaque to light but transparent to sound, is formed on a viewing screen by magnifying a side-band image in one direction by just the amount sufficient to correct the anamorphism.

The configuration considered (see Figure 1) is quite simple. In its most elementary form, it consists of only a laser, laser beam forming optics and a cylindrical lens in front of a viewing screen. There is also a water volume between lenses (which receives sound reflected from the object viewed) which for best performance must be kept free of particles which would scatter light onto the image plane.

The acousto-optical imaging system provides very precise control on the plane which is imaged due to the wide-band characteristic of the system. Whereas the alternative employing a mechanical structure, namely a hydrophone, is necessarily a resonant structure, this imaging system simply employs a volume of water with an absorber on the far side. Consequently, the impulse response of this system will be shorter than that of an efficient transducer since an efficient transducer is a narrow band device. The impulse response of any receiver is inversely proportional to bandwidth and therefore, the impulse response is quite long for a narrow band transducer. Since output voltage is given by the convolution of input signal with the impulse response of the receiver, output at a given time is determined by inputs spread over a range of time. Sound arriving over a fairly wide interval in range will contribute to receiver output unless the receiver has an impulse response which is short in duration (consistent with a wide-band device). With a wide-band device, such as the acousto-optical imaging system, output at a given time will be determined by returns from a small interval in range. The plane of interest can be imaged at the exclusion of other nearby planes by simply illuminating the Bragg cell with a short burst of laser light at the time when sound from the plane of interest arrives. It should be possible to limit the range interval affecting an image to the smallest possible dimension with the Bragg imaging system. It has been experimentally demonstrated that this can be as small as 1/3 centimeter in our laboratory system. The precision to which a laser can be pulsed provides precise control of the range to range interval to be visualized using standard laser components.

Holograms can be simply formed with an acousto-optic imaging system by using laser light already present in a manner suitable for hologram formation. All of the advantages which have been found for optical holography should apply to this system when it is constructed to make holograms of

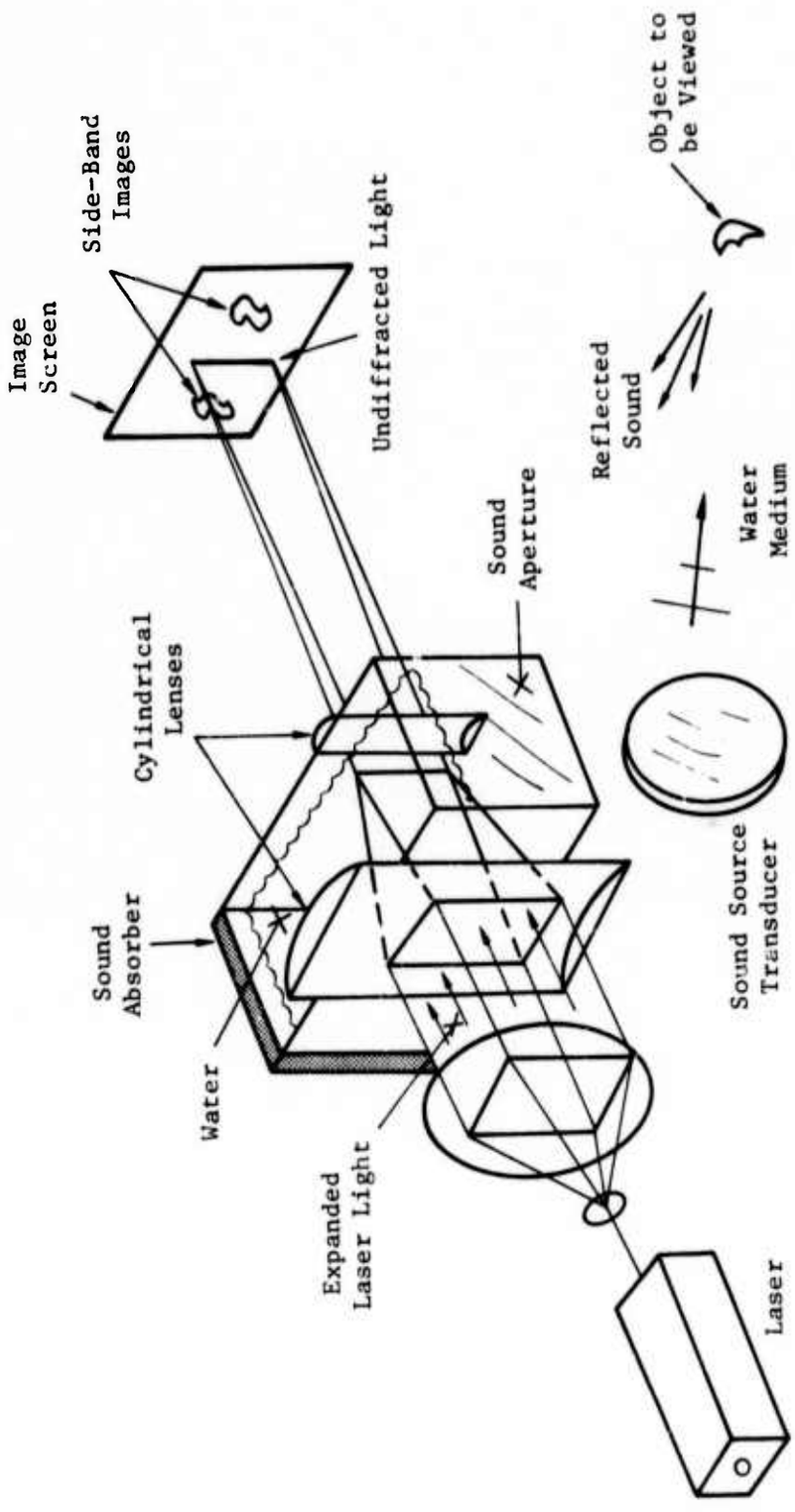

Figure 1: Elementary form of the acousto-optical imaging system.

the acoustic image. For example, in speckle reference holography, distortion introduced by the intervening medium can be removed from the final reconstructed image. Alternatively, contours revealing small movement of reflecting surfaces can be recorded holographically in very much the same way as this is achieved in double-exposure interferometry. Holographic recording of the side-band image has already been reported as useful for improving image quality by removing some of the effects of stray light which was not due to Bragg diffraction[7,8].

In the more standard acoustic system employing an acoustic reflector, the receiving hydrophones are located ahead of the reflector at positions interferring with arriving sound. Sound subsequently reaching the reflector is disturbed and, therefore, reflector performance is degraded at the receiving transducer. In the Bragg imaging system, only a light beam is ahead of acoustic reflectors. Consequently, a sound wave passes freely to the acoustic reflector and is returned to the interaction volume without distortion, giving the reflector maximum possible performance.

As already mentioned, the Bragg receiving system does not employ a resonant structure and is, therefore, inherently a wide band system. This makes it possible to use one system with operating frequencies spread over a broad range of frequencies. A single system can simultaneously receive sound of both low frequency and also very high frequency. This feature could be important in applications where the objective only requires rather poor resolution when the object is at long range with increased resolution at short ranges. Because of the attenuation properties of the sea, a long range capability requires the use of low frequencies and a short range capability allows the use of high frequencies where maximum resolution is achievable.

Both amplitude and phase of sound arriving at the Bragg cell is transferred to light forming the side band image. This provides the information necessary for later data reduction in cases where object complexity requires excessive computation for quality image formation.

The demonstrated sensitivity of the Bragg imaging system has proven to be equal to or better than a high quality narrow-band hydrophone. Moreover, theory predicts it should be possible to obtain a sensitivity determined only by noise in the form of sound waves arriving within the effective receiving aperture of the Bragg imaging system. Maximum sensitivity is possible by using optical heterodyning to pick up the image signal. This can be done in an optimum manner by using the dual frequency heterodyne scheme described in the first interim report[1].

2.0 REVIEW OF BASIC WORKING PRINCIPLES

Theory essential to understanding experimental results as well as requirements for improvements in performance are presented in this section.

Sound waves within a liquid (or solid) modify the refractive index due to compaction and rarefaction associated with internal pressure changes intrinsic to sound. The time average of the effect is analogous to a phase only thick hologram. As with the hologram, an image can be formed by illuminating the hologram with coherent light. A major difference between acousto-optical imaging and reconstruction of a hologram is that the acousto-optical system operates in real time. That is, the object which is visualized is present at the same time sound waves are reflected from or passing through the object. (This viewpoint of a basic working principle should not be confused with the formation of holograms in light emerging from the Bragg cell.)

2.1 Imaging Principles

Objects illuminated with sound produce (by reflection or scatter) a wave pattern completely analogous to the wave pattern reflected from visually viewed objects. Just as objects visually observed may be described by a distribution of plane waves of light, it is also convenient to describe sound reflected from insonified objects by a distribution of plane waves of sound. This viewpoint simplifies the analysis of acousto-optical imaging systems since individual plane waves can be considered separately. In order to understand acousto-optical imaging it is only necessary to observe the relation between each individual plane wave in the sound field and the resulting plane wave forming the image in the light field. An essential requirement is that each individual plane wave component in the sound field diffract one and only one plane wave component of light onto the image plane. This is the case in the acousto-optical imaging system considered here. It happens that significant light is diffracted by a plane wave of sound only when a plane wave component of light is present with a propagation vector at nearly right angles to the propagation vector for the sound.[1]

Formation of a high quality image from a sound field depends on the existence of light over a range of directions so that each plane wave component in the sound field will be replicated. Plane wave components in a sound field which are absent, of course, do not affect the light, and components in the sound field which find no light moving at the right angles for interaction would also be absent from diffracted light. An undistorted image is formed only if all components in the sound field defining the insonified image diffract light with the proper phase onto the image screen. In order to provide light necessary to interact with all plane waves of sound of interest, the acousto-optic cell is illuminated by cylindrically covergent light. There is then a continuum of light rays describing the light field. An alternate scheme uses spherically convergent light to provide a continuum of rays. In either scheme, a range of sound field vectors will encounter light satisfying the right angle condition. The cylindrically convergent light pattern has been found to be much superior at low sound frequencies and was used exclusively for all results reported here.

Any object can be thought of as a collection of points. The imaging of an arbitrary object can be understood by considering the imaging of one point. An object in the form of a point source can be considered as the superposition of a uniform distribution of plane waves. These plane waves diverge from that point. The wave vectors describing each plane wave then appear as rays. These rays are no different than rays used in geometric optics. Of course, the interpretation differs. This view simplifies estimation of the resolution capabilities of the system and estimates which follow from this viewpoint are consistent with more sophisticated theory. For example, consider a ray drawn from a point on the object which is reflecting sound back to the imaging system. Sound related to such a ray will not cause light to be diffracted to the image if it terminates outside the region where the acousto-optic interaction takes place. The acoustic receiving aperture can be no larger than the physical size of the dimensions of the region illuminated by laser light which also receives reflected sound. The effective aperture can be as large as the physical aperture by providing

a light field containing plane wave components in the light which have proper geometry for interacting with all sound wave components related to rays intersecting the light column. For example, the effective receiving aperture would be smaller than the physical aperture if the light wedge is confined to an angular extent which is less than the angle which subtends the physical aperture. The angle subtending the physical aperture would be measured in the plane in which the light wedge angle would be measured. Conversely, the presence of light within a larger wedge angle would be of no consequence other than possible degradation effects resulting from additional light that might be scattered onto the image plane due to Tyndall scattering.

2.2 Sensitivity

Except for stray light falling on the image plane, only incoming sound can produce image light. The acousto-optical system would be extremely sensitive if only light due to incident sound arrives on the image screen. Two-dimensional potential sources of unwanted light are due to diffraction from light illuminating the sound interaction volume. Light may be diffracted onto the image screen due to diffraction caused by the limited aperture thru which this light arrives. Additionally, as few as just one stray particle within light illuminating the interaction region or attached to optical surfaces will scatter a very significant amount of light when cell illumination light is quite intense. Since system sensitivity is proportional to intensity of illumination light,[9] these mechanisms can severely degrade maximum sensitivity of the system. Continual filtering of water can be expected to keep the interaction volume free of particles and lens surfaces can be kept clean (at least in principle). Diffraction from the aperture admitting laser light, or other light stop that might diffract light onto the image plane, can be made negligible by inserting the stop so as to place the sideband image in the shadow of a single edge as illustrated in Figure 2. The opposite side of the illuminating light column would be left in the form generated by the laser and beam expanding optics (probably Gaussian). It will be assumed that the edge of light opposite the edge with the stop is sufficiently distant to be considered infinite.

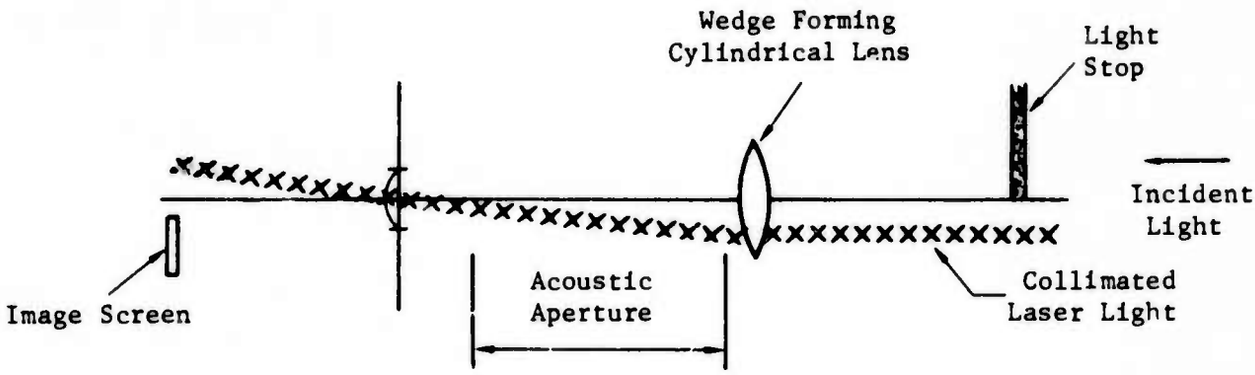

Figure 2: Beam forming optics which keep the image plane free of light due to edge diffraction.

To understand why the optical system in Figure 2 leaves the image screen free of light due to edge diffraction, note the image of the light stop could be reproduced on a plane near the image screen. To see this from an analytic viewpoint, note that the light pattern at the back focal plane of a lens is the Fourier transform of the light pattern in the front focal plane of the lens.[10] The light field in the front focal plane is just adjacent to the light stop (light is moving from right to left). When the acoustic image is in the column of cell illumination light the anamorphic image is opposite the focal plane of the lens on the right in Figure 2.[11] The lens on the left simply magnifies the light pattern when this lens and the image screen are correctly positioned. The light pattern falling on the image screen when no sound is present is then in the form of the Fourier transform of light passing a straight edge. This corresponds to the Fraunhofer diffraction pattern which is well known as the shadow of a straight edge (see Figure 3).[12] The image screen is located behind the image of the stop. Except for vignetting, which can be made negligible, the use of the light stop as illustrated totally prevents diffraction from edges from adding to light falling upon the image screen positioned to receive only one sideband image. If a second straight edge is used as a light stop and positioned opposite the straight edge in Figure 2 so that illuminating light is admitted thru a sharp edged aperture, diffracted

Figure 3: Shadow of a straight edge.

light would fall on the image screen due to this additional straight edge. This happens because the diffraction effects of the edge are seen on only one side of an edge (the light side) and with two edges as postulated effects are not completely excluded from any region. These observations have been confirmed in our laboratory experiments.

A well designed system which is free of scattering particles would have maximum possible sensitivity but one irreducible mechanism remains which scatters light onto the image plane. This mechanism is due to irreducible small fluctuations in the refractive index of any pure liquid (or solid). The scattering of light by irreducible fluctuations in the refractive index of a liquid, at temperatures above absolute zero, has been studied by several investigators over a period of more than sixty years. These investigators have considered the fluctuations to be due either to media density and temperature variations or to entropy and isentropic pressure variations (sound waves). With the former point of view, fluctuations are related to variations in temperature at constant density plus variations in density at constant temperature. With the latter point of view, dielectric constant (and concomitantly refractive index) variations are expanded into a term giving the contribution due to fluctuations in entropy (or temperature) at constant pressure plus the contribution due to the fluctuations in pressure (or density) at constant entropy. The two viewpoints are basically different in the parameter that is considered constant.

The latter point of view (giving a constant entropy plus a constant pressure term) leads to the separation of total scatter into two phenomenologically different terms. One term expresses the light scattered by propagating fluctuations in the dielectric constant and the other term expresses the light scattered by non-propagating fluctuations. The propagating fluctuations are called thermal phonons (sound waves). Scatter due to these fluctuations was considered in detail by Brillouin in 1922[13] and is now called Brillouin scatter. The term due to non-propagating fluctuations relates to scattered light which is called Rayleigh scatter by many authors. Rayleigh scatter from water is negligible relative to Brillouin scatter. Brillouin scatter is due to thermal phonons. Thermal phonons are received by the standard hydrophone as thermal noise. Thermal phonons can be considered as simply a continuum of low amplitude sound waves having a continuum of frequencies.

2.2.1 Light Diffracted by the Sound Signal

The significance of light scattered by random fluctuations in the light/sound interaction medium can be best determined with reference to the threshold of sound intensity required to overcome image noise. In order to determine this threshold, the relationship between sound intensity and image light intensity must be determined.

The relation between diffracted light intensity and the intensity of a sound wave in the form of a plane wave has been investigated by several authors.[15] A summary of work published prior to 1953 is included in a basic reference by Bhatia and Noble[16] along with an extensive theory determining Bragg diffraction of light into many possible orders assuming a wide range in the angles of incidence of illuminating light. At the lower frequencies of interest in this study ($\sim$ 500 KHz), diffraction must be considered to be Raman-Nath.[1] Interaction of any light ray is limited to an interval much less than a wavelength of sound unless excessively large ($\sim$ 100 meters) interaction regions are employed. Raman and Nath showed that the maximum intensity of diffracted light occurred when an incident plane wave of sound has

a propagation vector at right angles to the propagation vector for a plane wave of light.[17] This result applies under the Raman-Nath assumption, which is

$$\lambda_1 d << \Lambda^2 \tag{1}$$

where λ_1 = wavelength of light in the interaction medium
d = length of the interaction measured along the light path
Λ = wavelength of sound in the interaction medium

Under the right angle condition, the intensity of light diffracted into the n^{th} order is given by[17]

$$I_n = I_o J_n^2 \left[\frac{2\pi}{\lambda} \left(\frac{\partial n}{\partial P} \right)_s P \, d \right] \tag{2}$$

where I_o = intensity of incident light (in the form of a plane wave)
$J_n[\ ]$ = the ordinary Bessel function of order n
$\left(\frac{\partial n}{\partial P} \right)_s$ = adiabatic piezo-optic coefficient
P = peak pressure of the acoustic wave in the medium
d = length of the interaction measured in the direction of light propagation

Although the analysis of Raman and Nath also covered the case where diffraction can be considered to be Bragg diffraction ($\lambda_1 d > 2\Lambda^2$), the result from analysis published by Bhatia and Noble for Bragg diffraction will be compared with the result from Raman and Nath's analysis. Bhatia and Noble[16] show that the first order diffracted plane wave will have an intensity given by

$$I_{-1} = \frac{1}{4} \frac{I_o \delta^2 \sigma^2}{\left(\xi - \frac{1}{2} \right)^2 + \frac{1}{4} \delta^2 \sigma^2} \sin^2 \left(\beta d \left\{ \left(\xi - \frac{1}{2} \right)^2 + \frac{1}{4} \delta^2 \sigma^2 \right\}^{1/2} \right) \tag{3}$$

where $\sigma = (n^2 + 2)(n^2 - 1)/(3n)$

$\delta = \Delta(\Lambda/\lambda)^2$

Δ = peak fractional change in the density of the medium

$\xi = (\Lambda/\lambda)\sin\theta$

θ = angle between the propagation vectors of the incident light and sound wave (considered plane), respectively

Λ = wavelength of sound

λ = wavelength of incident light in vacuum

$\beta = \pi\lambda/(\Lambda^2)$

d = length of light/sound interaction measured along the propagation vector of incident light

This equation holds only when $\xi \simeq \frac{1}{2}$ and $\delta << 1$. Note that the Bragg condition is defined by $\xi = \frac{1}{2}$. The condition that $\delta << 1$ is consistent with the low intensities of sound that are of interest in this threshold study. The argument of the sine function in Eq. (3) is small at $\xi = \frac{1}{2}$ when threshold conditions apply ($\beta d\delta\sigma << 1$). The form of Eq. (3) of interest in this study then follows from the small angle approximation. For threshold analysis, Eq. (3) becomes

$$I_{-1} = \frac{I_o}{4}\beta^2 d^2 \sigma^2 \delta^2 \tag{4}$$

The average power density (watts/m^2) carried by an acoustic plane wave was used to express the result of Raman and Nath. It is also required to put Eq. (4) in a more useful form. The average power of a plane wave in liquid is[20]

$$I_s = P^2/(2Z_a) \tag{5}$$

where P = the peak pressure of the wave

$= Z_a(v_s\Delta)$

Z_a = acoustic impedance

$= \rho v_s$ for a liquid

ρ = density of the medium

v_s = velocity of the sound wave in the medium

The peak fractional change in density follows from Eq. (5). It is

$$\Delta = \left[2I_s/(\rho v_s^3)\right]^{1/2} \tag{6}$$

so that

$$\delta^2 = \frac{2I_s}{\rho v_s^3}\left(\frac{\Lambda}{\lambda}\right)^4 \tag{7}$$

(U) The near Bragg condition $\left(\xi \simeq \frac{1}{2}\right)$ must be satisfied for Eq. (4) to hold. It is well known that the intensity of diffracted light rapidly approaches zero as the incidence angle deviates from the direction which either the Bragg condition or right angle condition for Raman-Nath diffraction. A given spatial spectral component (a plane wave) in the sound field will therefore produce a unique related spatial spectral component in the diffracted light for both the Raman-Nath and Bragg regimes. It is interesting to note that the intensity of diffracted light under both Raman-Nath and Bragg conditions is the same when the sound level is near threshold conditions. To see this, note that for Raman-Nath conditions the diffracted light intensity follows from the small argument approximation of the Bessel function which is $J_1(Z) \cong Z/2$ for $Z << 1$. At threshold conditions the intensity of light diffracted into the first order is (from Eq. (2`)

$$I_1 = \frac{\pi^2}{\lambda^2}\left[\left(\frac{\partial n}{\partial P}\right)_s\right]^2 p^2 d^2 I_o \tag{8}$$

It can be shown that the variation in refractive index with density at constant entropy is given by[9]

$$\left(\frac{\partial n}{\partial \rho}\right)_s = (n^2 + 2)(n^2 - 1)/(6\rho n)$$

Using

$$\left(\frac{\partial n}{\partial P}\right)_s = \left(\frac{\partial n}{\partial \rho}\right)_s \left(\frac{\partial \rho}{\partial P}\right)_s = \left(\frac{\partial n}{\partial \rho}\right)_s \frac{1}{V_s^2} \tag{9}$$

Equation (9) becomes

$$\left(\frac{\partial n}{\partial P}\right)_s = (n^2 + 2)(n^2 - 1)/(6n\rho v_s^2) \tag{10}$$

The first order diffracted light intensity is then (using Eqs. (8) and (10))

$$I_1 = \pi^2 \left(\frac{d}{\lambda}\right)^2 \sigma^2 \frac{\tau_s I_c}{2\rho v_s^3} \tag{11}$$

Substitution of applicable definitions into Eq. (4) shows that the intensity of light in a lst order sideband under Bragg conditions for low amplitude sound is given by the same expression as that for Raman-Nath conditions, Eq. (11). Equation (11) will therefore be used to relate the intensities of the spatial spectrum of the distribution describing the sound field.

Equation (11) applies to incident light in the form of a uniform plane wave. The system considered here is illuminated by a cylindrically convergent wedge of light with the convergence axis directed vertically. The interacting intensity of plane wave components within incident light must be determined in order to use Eq. (11). The interacting plane wave of sound on which Eq. (11) is based is of limited extent (d units wide). It is the width of the interaction region (d) which determines the incident light intensity available for interaction with an infinite plane wave component of the sound field.

The x-axis is taken normal to a vertical plane which contains the axis of convergence and which bisects the wedge of light. The system considered uses illumination with a uniform spatial spectrum between x-directed spatial frequency limits given by

$$f_{xm} = \frac{\pm \sin\alpha_m}{\lambda} \tag{12}$$

where α_m = one half the angular width of the wedge of illuminating light

The Bragg imaging system would, ideally, be illuminated with light distributed uniformly over spatial frequencies within limits corresponding to the angular width of the "wedge" of illuminating light. We shall consider this to be the case since any variation from a uniform distribution would introduce amplitude aberrations.

The question to be answered now is "how much incident light power is involved in producing an image (neglecting noise) of a plane wave of sound which is d units in width?" Observe that a uniform plane wave of sound of width d in the horizontal direction (and infinite height) will produce an image (without any lens) of width equal to $\lambda d/(n\Lambda)$ in media of refractive index n. Now the horizontal directed spatial spectrum of light forming the width pattern is the same as the spatial spectrum within interacting incident light.[22] The (spatial) spectral amplitude density of interacting incident light involved in forming an image of width, $\lambda d/(n\Lambda)$, can be written

$$u'(f_h) = \left(\frac{d\lambda}{n\Lambda}\right) \frac{\sin \pi f_h \left(\frac{\lambda d}{n\Lambda}\right)}{\pi f_h \left(\frac{\lambda d}{n\Lambda}\right)} u_o \tag{13}$$

where u_o = amplitude of the incident plane wave which will produce $u'(f_h)$ if the incident plane wave of amplitude u_o were incident on a slit of width $\lambda d/(n\Lambda)$

f_h = the horizontal directed spatial frequency directed so as to yield a symmetrical distribution. The reference direction for f_h will vary with the particular sound field component considered

The intensity of an incident plane wave of amplitude u_o is

$$I_o = |u_o|^2/2 \tag{14}$$

To determine I_o, (the intensity available for interaction) expand the entire uniform spatial spectrum contained within incident light into equally spaced components of the same form as Eq. (13). Thus, we can write[18] for the total amplitude spatial spectrum in cell illumination

$$L(f) = \frac{u_o \lambda d}{\Lambda} \sum_m \text{Sinc} \quad (X_s f - m)$$

$$m = \ldots -2, -1, 0, 1, 2, \ldots$$

where $|m|$ = an integer $\leq N/2$

$X_s = \frac{\lambda d}{n\Lambda}$

$\text{Sinc}(t) = \frac{\sin \pi t}{\pi t}$

N is defined by Eq. (15)

The interval between neighboring sinc functions is $1/X_s = n\Lambda/(\lambda d)$. The total number of "samples" within the spatial bandspread of incident light, $(2\sin\alpha_m$, , is

$$N = \frac{n2\sin\alpha_m}{\lambda} \frac{\lambda d}{n\Lambda} = \frac{2d\sin\alpha_m}{\Lambda} \tag{15}$$

where $\frac{\sin\alpha_m}{\lambda}$ = the maximum spatial frequency in incident light

The power in each "sample" per unit height is just the integral of the square of Eq. (13) over all spatial frequencies. It is

$$W_1 = \int_{-\infty}^{\infty} \frac{\left|u'(f_h)\right|^2}{2} df_h = \frac{u_o^2 \lambda^2 d^2}{n^2 \Lambda^2} \int_{-\infty}^{\infty} \frac{\sin^2 \pi f \frac{\lambda d}{n\Lambda}}{\left[\pi f \left(\frac{\lambda d}{n\Lambda}\right)\right]^2} df$$

The completed integral gives

$$W_1 = \frac{u_o^2}{2} \frac{\lambda d}{n\Lambda} = I_o \frac{\lambda d}{n\Lambda} \tag{16}$$

The total power per unit height of the wedge of incident light is (from Eqs. (15) and (16)).

$$P_e = NW_1 = \frac{2d^2 \lambda I_o \sin\alpha_m}{n\Lambda^2} \tag{17}$$

An incident plane wave of light of proper orientation and intensity, I_o, will produce the same image intensity as that which will appear when the cell is illuminated by a wedge of light with total power per unit height, P_e, if the sound field is uniform and of width d.

The equivalent intensity of each plane wave component in incident light which is available for interaction with a plane wave component of the sound field is (from Eq. (17))

$$I_o = \frac{n\Lambda^2 P_e}{2\lambda d^2 \sin\alpha_m} \tag{18}$$

The intensity of light in the image due to a more-or-less uniform source of sound of intensity, I, is therefore (from Eqs. (11) and (18))

$$I_{-1} = \frac{n^2\pi^2\sigma^2}{4\rho v_s^3} \frac{\Lambda^2}{\lambda^3} \frac{I_s P_e}{\sin\alpha_m} \tag{19}$$

In the system considered here, pure water is considered to exist everywhere within the light/sound interaction region. For pure water $\sigma = \frac{1}{n}$, $\rho v_s^3 = 3.38 \times 10^{12}$ watt/m^2 and $n = 1.33$. We shall assume an argon-ion laser operating at 4880Å is used to illuminate a water filled sound cell. For this case the diffracted light intensity (watts/cm^2) is

$$I_{-1w} \tilde{=} 8.3 \times 10^4 \Lambda^2 I_s P_e/\alpha_m \tag{20}$$

where I_s = sound intensity (w/cm^2)

P_e = power per unit height of the light wedge of illumination (w/cm)

Λ = sound wavelength in cm

Note that the intensity in an image which is magnified sufficiently to give the correct aspect ratio, which also is the same size as the object, will be reduced in intensity by the factor (λ/Λ). The intensity in the orthoscopic plane due to a uniform sound source of intensity I_s will then be

$$I_{-1f} = \frac{\pi^2}{4} \frac{n\sigma^2}{\rho v_s^3} \frac{\Lambda}{\lambda^2} \frac{I_s P_e}{\sin\alpha_m} \qquad (21)$$

In the case where the object is not a uniform distribution of sound, Eq. (21) expresses the intensity due to sound passing through only that part of the object which scatters sound into angles far less than the maximum angular aperture of interaction. In this case, the spatial frequency spectral intensity in scattered sound will be related to the spatial spectral intensity of light falling on the image in such a way that Eq. (21) will give the intensity of light at the applicable point in the image, if I_s is the sound intensity passing through the corresponding point of the object.

When the spatial spectral intensity is quite significant at spatial frequencies well above f_m, the intensity of light on the image is less than that given by Eq. (21). The image light intensity distribution in this case can be obtained by observing that Eq. (21) implies the Bragg imaging acts like a linear system (P_e is constant). The implications of the limited effective Bragg imaging system aperture on the image are expressed in terms of system resolution.

The present investigation does not include an objective as ambitious as that of using only sound already present in the sea to view an object in water too dirty to be observed with light. This is consistent with opaque object inspection since sound at intensities near cavitation is required to view the interior of opaque objects with enclosing material. Enclosing material typically introduces very significant attenuation. The only objects expected to introduce little attenuation are those specifically designed to be transparent.

2.2.2 Brillouin Scatter

Bragg diffraction (as parametric frequency conversion) is, ideally, a noiseless phenomenon. It "cannot be initiated by zero-field vibrations."[19]

However, diffraction due to coherent sound will be accompanied by Brillouin scatter. Brillouin scatter has been isolated as the irreducible source of noise limiting the sensitivity of Bragg imaging systems using a coherent sound source for object illumination.[9] Reference 9 shows that the intensity of Brillouin scattered light falling on the orthoscopic image plane of a Bragg imaging system operating at low sound frequencies is approximately

$$i_o(0) = \frac{\pi^2}{\lambda^3} \frac{\sigma^2 n^2 \gamma k T P_t \ell n(r_1/r_o)}{\rho V_s^2 \Lambda Y_o} \tag{22}$$

where λ = wavelength of illuminating light

Λ = wavelength of sound

i_o = light intensity

n = refracting index of the light/sound interaction medium

γ = ratio of isothermal to adiabatic compressibility (= 1.0066 for water)

ρ = density of the interaction medium

V_s = velocity of sound in the interaction medium

Y_o = a Bragg cell design parameter determined by distance to the image screen

k = Boltzmann's constant

T = equilibrium temperature

P_t = total power of the illuminating laser

r_1/r_o = ratio of (1) the radial distance between the Bragg cell boundary where illuminating light arrives first and the point of focus of this light to (2) the radial distance of the opposite boundary from the same point of focus. A small cell would typically be made with r_1/r_o equal to about 20

2.2.3 Signal Intensity for Fifty Percent Contrast in the Orthoscopic Plane

The sound signal level required to diffract light of intensity equal to the intensity of Brillouin scatter is a useful index for the threshold of sound required to overcome the illumination due to the thermal phonons. This would be a problem in direct viewing by the human eye where a brightness control is not available. For this case, image contrast will equal 50%. The corresponding signal level is determined by setting Eq. (21) equal to Eq. (22). Solving for I_s from the resulting equation shows that the sound intensity required for 50% contrast in average intensity on the orthoscopic plane is

$$I_{suo} = \frac{4\sin\alpha_m}{\lambda\Lambda^2}\,\gamma kT\,\frac{nv_s L}{Y_o}\,\ell n(r_1/r_o) \tag{23}$$

Observe that the scattered light which falls on the orthoscopic plane will be spread over a band of frequencies defined by the scattering angles involved in all light falling on a point. To determine the maximum scattering angle in light reaching the midpoint of the orthoscopic plane, let the orthoscopic image be located at a distance from the interaction region given by Y_o. The vertical component of the scatter angle for scattered light reaching the orthoscopic image therefore cannot exceed $(L/2)/(Y_o)$ radian. The relation between the angle through which incident light is diffracted and frequency of the sound wave causing the diffraction is the same for both Raman-Nath and Bragg conditions at frequencies of interest here. When the scatter angle is small enough for the sine of the angle to be taken equal to this angle (expressed in radians), sound frequency which is related to a given scatter angle is

$$f(\theta) \tilde{=} \frac{V_s n\theta}{\lambda}\ \text{Hz} \quad \text{for } \theta << 1 \tag{24}$$

where θ = angle between propagation vectors of incident and diffracted light (radians)

From Eq. (24), we see that this restricts the temporal frequency bandwidth in scattered light falling on the orthoscopic plane to

$$B_o = \frac{4nv_s}{\lambda}\left(\frac{\theta}{2}\right) = \frac{nv_s L}{\lambda Y_o} \tag{25}$$

A resolution cell of the Bragg imaging system which has a large field of view in the z direction will be approximately equal to

$$A_r = \left(\frac{2}{3}\Lambda\right)\left(\frac{\Lambda}{2\sin\alpha_m}\right) = \frac{\Lambda^2}{3\sin\alpha_m} \tag{26}$$

where A_r = the aperture area of the transducer and therefore the resolution area

In terms of A_r and B_o, Eq. (23) can be written

$$I_{suo} = (4/3)\gamma\ell n(r_1/r_o)\,\frac{kTB_o}{A_r} \tag{27}$$

The thermal phonons producing Brillouin scatter move at random throughout the interaction medium and there is a noise-like sound intensity associated with them. Equation (27) is expressed in such a form as to emphasize this point. Recall that a transducer type of sound-detection system with bandwidth B_t will exhibit an equivalent input thermal noise intensity given by

$$I_{th} = \frac{kTB_t}{A_r} \tag{28}$$

If we consider thermal noise only, it is apparent that the Bragg imaging system approaches the sensitivity of a conventional noiseless electronic system of the same passband. (Note that this assumes a sufficient number of photons are collected in each resolution cell to make photon noise negligible.

In any electronic system, the bandwidth will naturally be many orders of magnitude less than the Bragg system bandwidth involved in scattering the light. Thus, an electronic system can be many orders

of magnitude more sensitive than a Bragg imaging system which accepts all light falling upon the anamorphic image plane. However, the Bragg system can be made sensitive to only light at frequencies in a narrow passband about the signal frequency by use of a light heterodyne system. If it is possible to limit the sensed passband to that of the electronic system, the Bragg system can be made to approach the theoretical sensitivity capability of a noiseless electronic system.

The fact that Eq. (27) differs from Eq. (28) by a geometrical factor implies that the number of thermal phonons scattering light into a resolution cell in the image is different from the number passing through a resolution cell in the water.

Equation (27) suggests that a few more thermal phonons scatter light into a resolution cell than pass through an area of size equal to a resolution cell in the sound field. How can this be? A clue is found by reference to Eq. (27). This equation implies that the minimum detectable signal varies with $\ell n(r_1/r_o)$. An increase in the size of the field of view will increase the noise level by a small amount. A plausible explanation for this is that a locus of points in the sound field will all contribute to forming one point in the image if a band of frequencies are present in the sound field.

To see that this is the case, consider the imaging of a wire with wire axis parallel to the z-axis. Imaging rules are then limited to positions in the x-y plane. Draw a line from the z-axis (convergence line of incident light) to any selected point in the image. The position of the wire object which will image at the selected image point must be located at the apex of an isosceles triangle with base consisting of the line connecting the z-axis to the selected imaging point.[4] A perpendicular bisector of the base of this triangle will pass through the apex of the triangle. The apex of all isosceles triangles (with the same base) will lie on this perpendicular bisector. The location of the apex is the location of the source which will image at the selected point. The Bragg angle determines which triangle defines the object location which will image at the selected point. It is that triangle with apex angle equal to twice the Bragg angle

which defines the image rules.[4] The Bragg angle is a function of wavelength. It is then clear that the object that will image at any selected point must be moved along the perpendicular bisector as the frequency (and therefore, wavelength) of the sound is varied. If a string of objects arranged along the defined perpendicular bisector are illuminated with sound containing a band of frequencies, the image of all these objects would be superimposed at the selected image point. One would then expect phonons passing through several resolution cells to contribure to the noise arriving in a selected resolution cell of the image. This is conservative of energy since phonons not actually passing through the point imaged can appear to pass through the same point in the image plane. That is, area presumed to be outside of the field of view can be thought of as the source region for the computed excess in thermal phonons tending to mask an image of a resolution cell.

The sound intensity required to diffract light to the orthoscopic image plane at an intensity equal to Brillouin scatter (from water) is

$$I_{suo} = \frac{3.2 \times 10^{-11}}{\lambda \Lambda^2} \left(\frac{L}{Y_o}\right) \ell n(r_1/r_2) \ \frac{\text{watts}}{\text{cm}^2} \qquad (29)$$

(Λ is expressed in cm)

2.2.4 Image Pickup by Optical Heterodyning

Performance of a Bragg imaging system can be enhanced by using a television camera tube or other photo sensor system together with a television monitor to display the image. As with all electronic devices, there is an internal source of noise within the image pickup device which, in some cases, will determine system sensitivity. It is well known that optical heterodyne or homodyne detection is capable of providing greater sensitivity than direct forms when coherent light is to be detected. This happens because gain is associated with the heterodyne process making the signal at the photodiode output sufficiently large to squelch other noise terms. A convenient way to implement heterodyne detection is to use the two frequency imaging system shown in Figure 4.

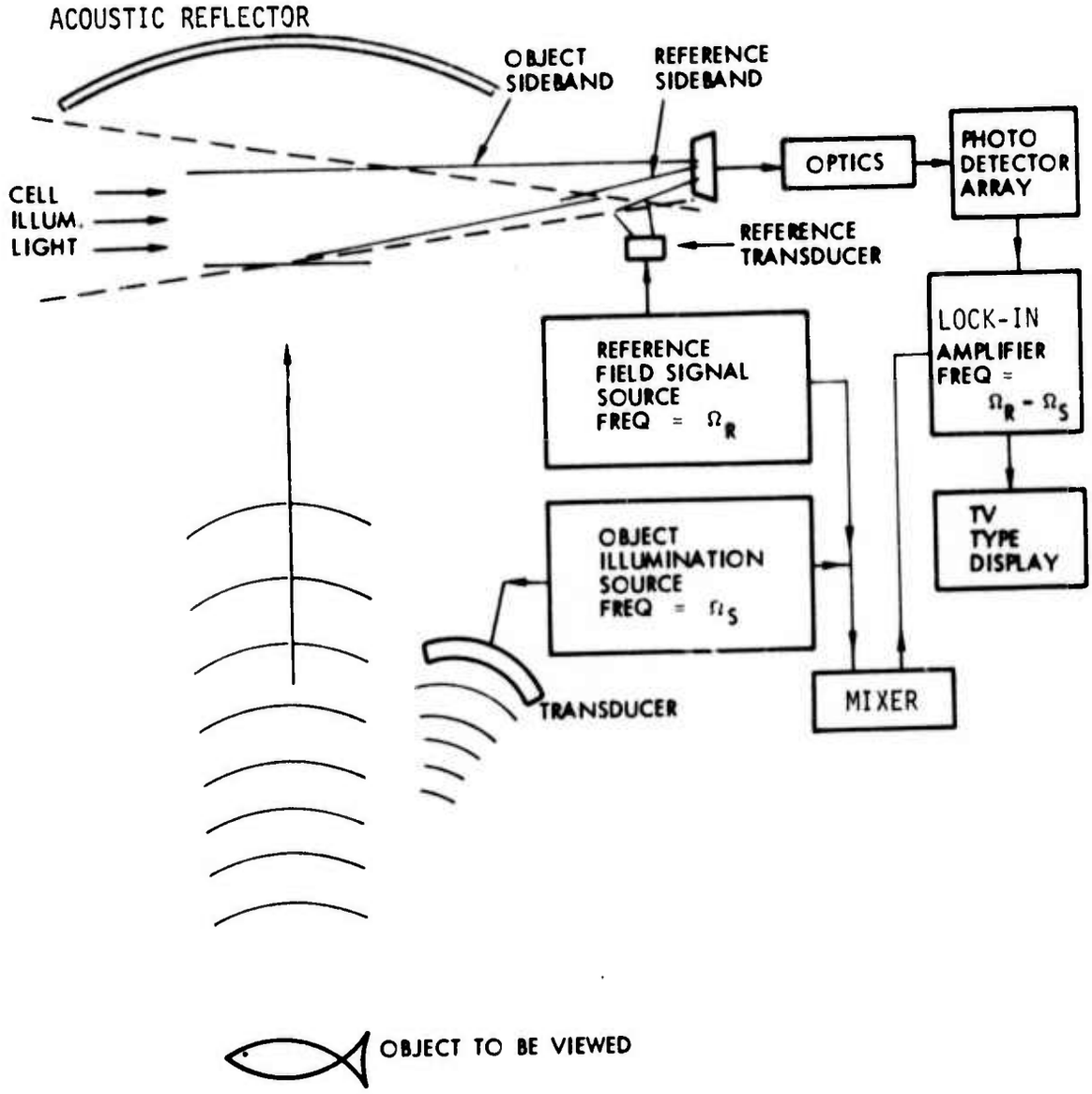

Figure 4: A double frequency heterodyning acousto-optical imaging system.

In this system, a reference transducer produces a uniform sound field which is subsequently imaged, producing a uniform "local oscillator" field.[1] Sound reflected from the object viewed produces an image that is superimposed upon the local oscillator field. The intensity of the local oscillator field can be adjusted to the optimum level by adjustment of the drive to the reference transducer. In this way, a very high power laser can be used to illuminate the light/sound interaction region while the local oscillator can be maintained at the optimum level. With a sufficiently strong local oscillator, the signal to noise ratio of an optical heterodyning system is given by[23]

$$\frac{S}{N} = \frac{q\, I_1\, A}{4\, h\nu\, B_o} \tag{30}$$

where I_1 = the image light intensity

A = the area of a resolution cell or detector area, whichever is smaller

B_o = the output bandwidth

h = Planck's constant

ν = frequency of the light

A signal-to-noise ratio of 5 is sufficient to produce a poor but visible image. Using S/N = 5 as a definition of threshold, system sensitivity is given by (from Eq. (30))

$$I_s^* = \frac{20\, h\nu\, B_o}{q\, A} \tag{31}$$

The sound level required to diffract this level of light onto the image plane is determined by equating Eq. (31) to Eq. (19). Threshold sensitivity for imaging sound with optical heterodyne pickup of image light is given by (from Eqs. (19) and (31))

$$I_s^* = \frac{80\, hc\, B_o\, \rho V_s^3\, \lambda^2 \alpha_m}{\pi^2\, q\, A \sigma^2\, \Lambda^2 P_e\, n} \tag{32}$$

The last result is based upon an image which is full size. A reasonable value for the resolution area, A, is four sound wavelengths in the vertical direction by Λ/α_m in the horizontal direction or $A \tilde{=} 4\Lambda^2/\alpha_m$. The value of A, applicable to any specific system, may vary and will depend upon acoustic reflectors or lenses which may be used. For example, in laboratory experiments reported in the report for Phase I, the detector area was smaller than a resolution cell size but magnification was not changed as the frequency was changed. As a result, observed sensitivity should be proportional to the square of frequency (inversely proportional to wavelength squared). In order to provide sensitivity estimates, consider an optical heterodyning system which converges all light within a resolution cell onto a detector. The collection area for a full size image will be assumed to be

$$A = 4\Lambda^2/\alpha_m$$

Using this assumption and $\alpha_m = 1/12$ with $\lambda = .5145$ μm, Eq. (32) becomes

$$I_{sl}^{*} = 3.56 \times 10^{-25} \frac{B_o}{q\, P_e\, \Lambda^4} \quad \text{watts/cm}^2 \tag{33}$$

where B_o = system bandwidth Hz

P_e = laser power per unit height of the wedge watts/cm

Λ = sound wavelength in centimeter

q = quantum efficiency

An example of a typical case, let $P_e = 1$ watt/cm, $q = .75$ and $B_o = 1$ Hz. At a sound frequency of 500 KHz, $\Lambda = .3$ cm, a threshold sensitivity of 5.9×10^{-23} watts/cm^2 is theoretically possible. This corresponds to about -100 db.

3.0 PROJECTED RANGE PERFORMANCE SONAR

Performance range was presented in the previous interim report on this project. Recent improvement in the acousto-optical system and calibration of transducers used have shown that the acousto-optical system is more sensitive than previously reported. Calculation of maximum theoretical sensitivity has also been recently completed as presented in the previous section. Consequently, maximum operating range is greater than previously published estimates. For this reason, range calculations have been repeated and this section has been revised based on both theory and new experimental results.

3.1 Sensitivity Experiments

New experiments were performed to measure the maximum sensitivity achievable with the TRW acousto-optical dual-frequency system. Sensitivity of the dual-frequency heterodyning system shown in Figure 4, was obtained by directing image light to a photodetector which drives a phase sensitive lock-in amplifier. The lock-in amplifier approach makes amplification with a pass-band of only 1 Hertz particularly convenient. For these measurements, a small sound source was placed at a distance of 15 feet to allow sound to become more planar over most of the 4 foot interaction length of the light/sound interaction region. A cylindrical acoustic reflector of .46 meter with power direction vertical was used to capture and return sound within the 6 inch height of the cell illumination light.

Two major factors contribute to the difference between current sensitivity measurements and those reported in Ref. 1. An NRL/NSRD E27 calibrated transducer was employed to measure the acoustic pressure at the aperture of the acousto-optical imaging system (an efficiency of 100% conversion was previously assumed) and an acoustic reflector replaced the acoustic lens previously employed. These modifications resulted in a received sensitivity at 500 KHz of 1.46×10^{-16} watts/cm^2. This is equivalent to an echo level of -36.6 db referenced to the intensity of a plane wave of rms pressure of 1 dyne/cm^2. This sensitivity represents an improvement of 34.3 db over the value reported in Ref. 1. If the directivity of the reflector, 16 db, is removed the Bragg cell receiver sensitivity is -20 db re 1 μbar at 500 KHz frequency.

3.2 Range Calculations

Predicted ranges for the TRW Acousto-Optical Imaging System have been calculated as a function of temperature, salinity, depth, frequency and particulate concentration, target strength and field of view. This has been accomplished using a computer program[1] which solves the basic two way transmission sonar equations using system sensitivity as determined by theory and also as observed experimentally. Reverberations were neglected since inclusion would make it quite difficult to compare this system with alternatives. Additionally, imaging implies that sound arriving from different directions due to reflections at the same range will show up in different parts of the image and therefore, should not degrade operating range. Maximum operating range is determined by the sonar equation which is[20]

$$SL - 2TL + TS = EL \tag{34}$$

where SL = source level

$TL = 20 \log R + \alpha R \times 10^{-3} + \alpha_p R$

R = range

α = logarithmic absorption coefficient

α_p = logarithmic absorption coefficient due to particle concentration

TS = target strength = 0 db

EL = minimum detectable echo

The source level was assumed to be 10 Kilowatts with the transmitting directivity index of a transducer illuminating a 90° sector.

The logarithmic absorption coefficient, α, was calculated using the equation of Schulkin and Marsh (Ref. 21)

$$\alpha = ASf_T f^2/(f_T^2 + f^2) + Bf^2/f_T$$

$$f_T = 21.9 \times 10^6 - 1520/(T + 273) \tag{35}$$

where A,B = constants

S = salinity in parts per thousand

f = acoustic frequency in kilohertz

T = temperature in degrees centigrade

α_p was calculated using the equation[21]

$$2\alpha_p = C\left[k^4a^3/3 + k(\sigma_1 - 1)^2 S/\left(S^2 + (\sigma_1 + \tau)^2\right)\right] \quad (36)$$

where C = total volume concentration of the particles

k = wave number of the acoustic signal

a = effective particle radius = 4 microns

σ_1 = particle density/water density = 2.65

$S = 9/4\beta a\ (1 + 1/\beta a)$

$\beta = (\omega/2\mu)^{1/2}$

ω = angular frequency

μ = kinematic fluid viscosity

$\tau = 1/2 + 9/4\beta a$

The minimum detectable echo which was used to determine maximum theoretical range is given by Eq. (33). When expressed in terms of minimum detectable echo level (referenced to 6.5×10^{-13} w/cm^2), Eq. (33) can be written

$$EL = -(121 + 40 \log_{10}\Lambda) \quad (37)$$

where Λ is the wavelength expressed in centimeters.

After substitution of Eqs. (35), (36) and (37) into Eq. (34), the resulting equation for a 10 KW source level was solved for range using the bi-sectional method of iteration. The result for 0 db and -40 db target strength appears in Figure 5.

Maximum range with sensitivity no greater than experimental observations was also calculated. The minimum detectable echo was based upon the best that has been experimentally determined from the most recent measurements using the laboratory acousto-optical imaging

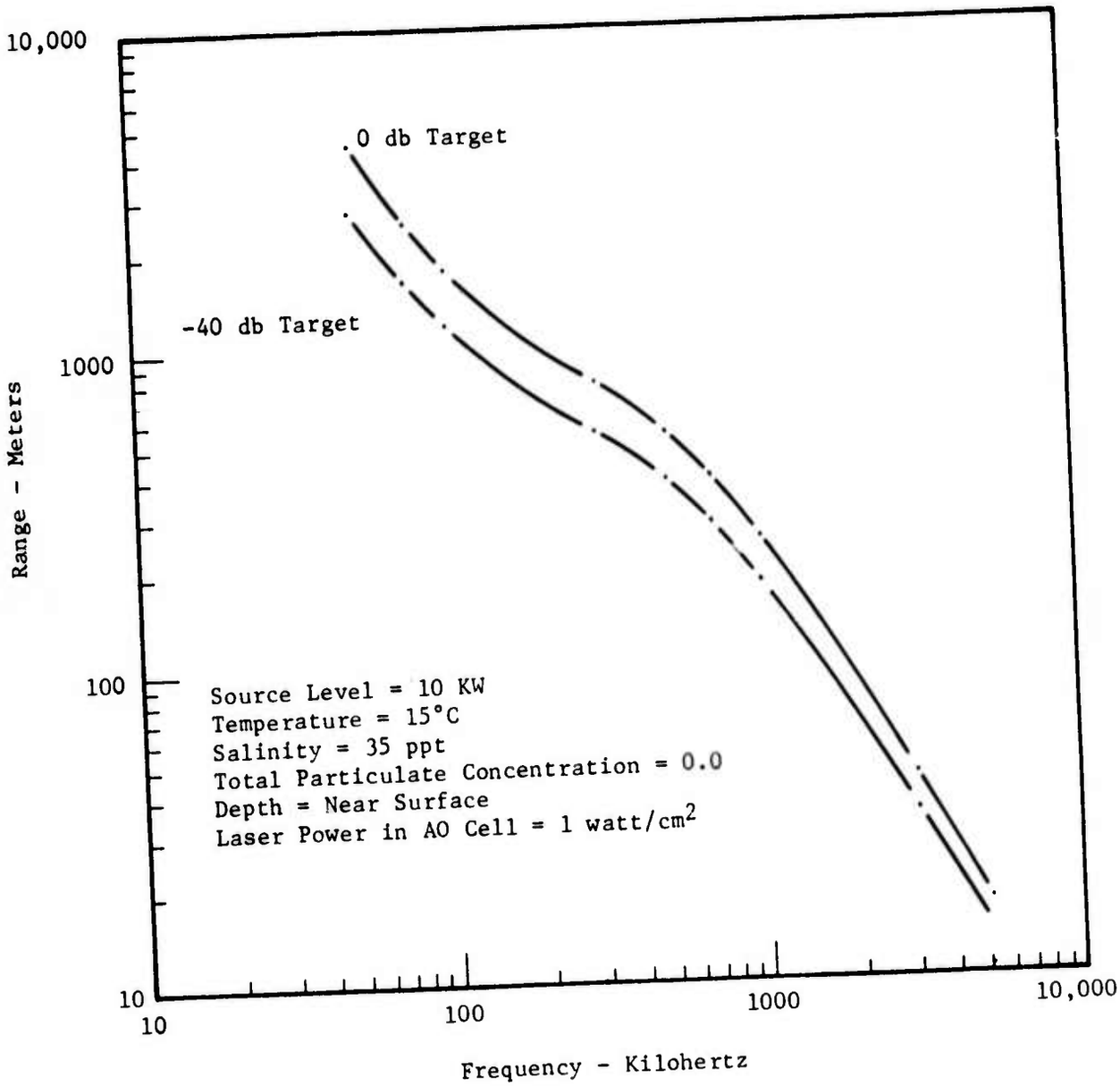

Figure 5: Maximum theoretical range for operation in the reflection mode. (U)

system. After substitution of Eqs. (35) and (36) into the sonar equation for two way transmission, the equation was again solved for range. The result appears in the following figures. Figure 6 is a plot of range vs. frequency with depth as a parameter. This figure shows that range has a very weak dependence on depth for the operating depths and frequencies which would be employed by the TRW Acousto-Optical Imaging System. The effect of salinity on system performance appears in Figure 7, which shows a maximum range variation of about 25 percent over extreme salinity changes. Figures 8 and 9 show the effects of volume particle concentration on range. The first figure displays a curve family for range vs. particulate volume concentration with frequency as a parameter. The second figure is the family of curves for range vs. frequency with particulate volume concentration as a parameter. Both of these curve families reveal an extreme reduction in range as particulate concentration increases. The plots of range as a function of temperature with frequency as a parameter and range as a function of frequency with temperature as a parameter are shown in Figures 10a and 10b, respectively. A 10 degree centigrade change in temperature can result in a maximum variation of about 30 percent in range. All of the above plots reveal the extreme effect of frequency on range for any acoustic system. Range is most strongly dependent on the variables of frequency and particulate concentration. However, any acousto-optical imaging system would have to be designed with regard for the application and environmental effects of all these parameters.

The new resolution measurements described in the next section indicate that the system is capable of operation at the theoretical acoustic limit. Thus, the resolution is limited only by the aperture dimension and the system trade-off of acoustic frequency and maximum range. A family of curves relating azimuth resolution to acoustic frequency with aperture dimension as a parameter is shown in Figure 11.

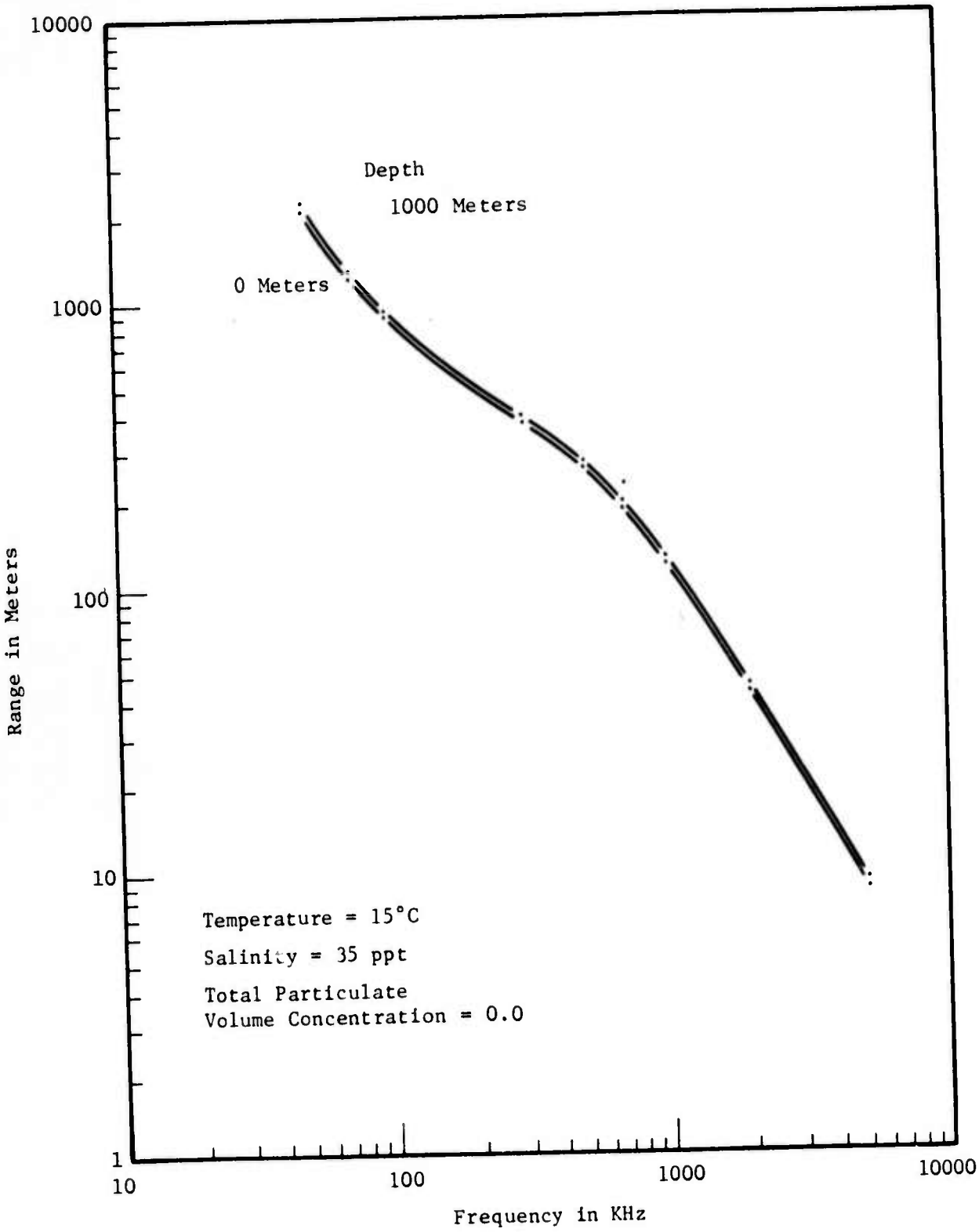

Figure 6: Dependence of range as a function of frequency with depth as a parameter.

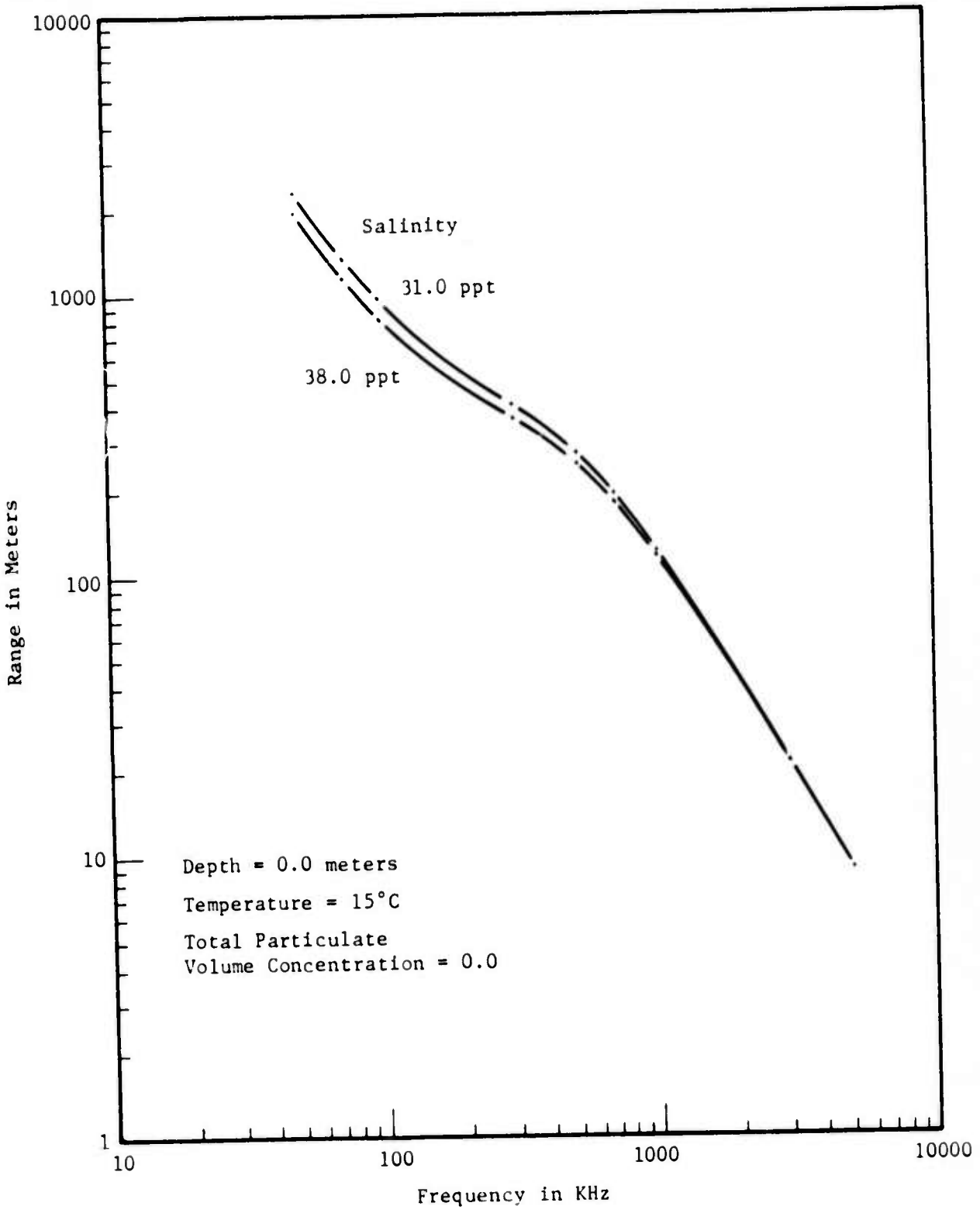

Figure 7: Dependence of range on frequency with salinity as a parameter.

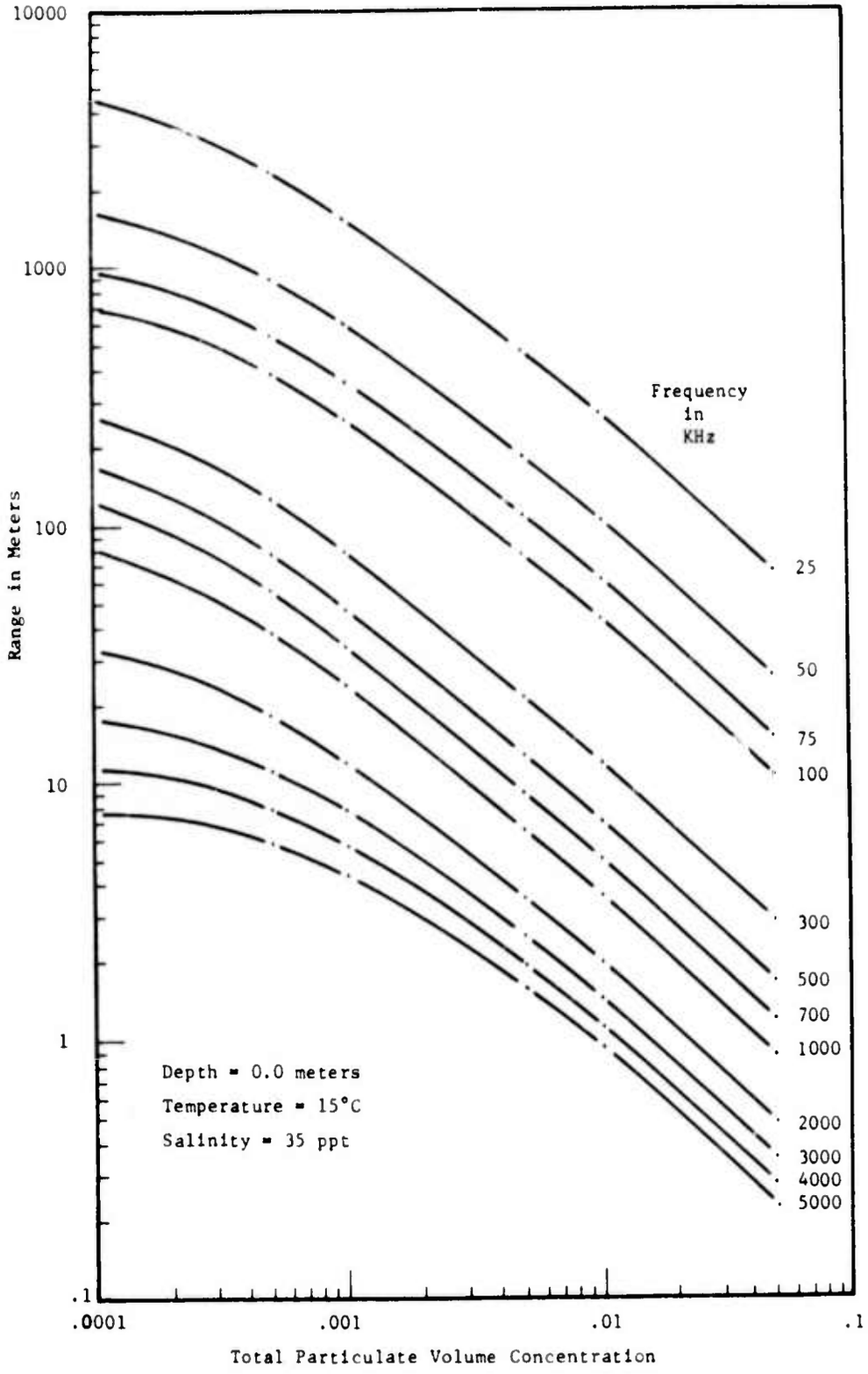

Figure 8: Range capability under dirty water conditions.

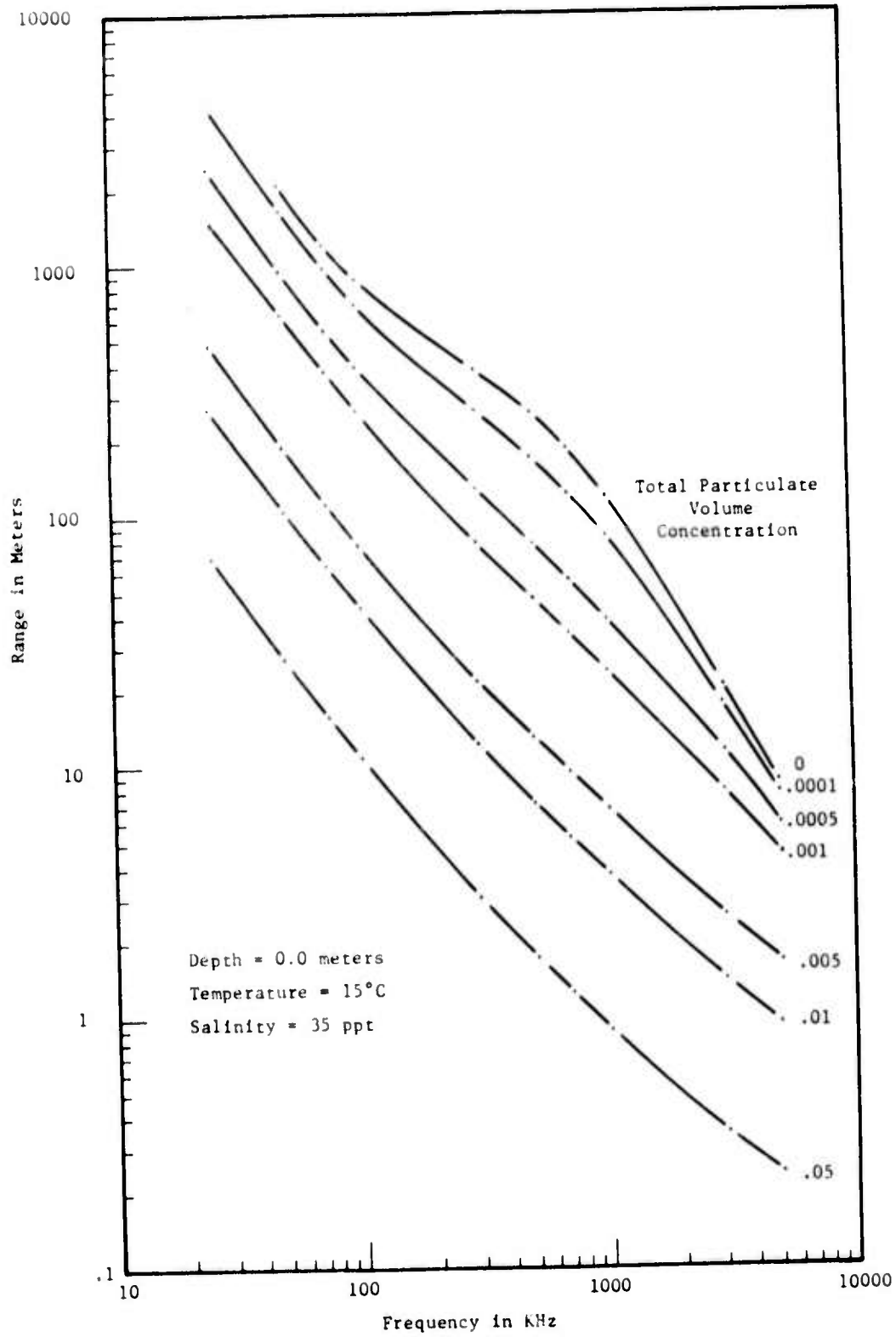

Figure 9: Dependence of range on frequency with particulate volume concentration as a parameter. (U)

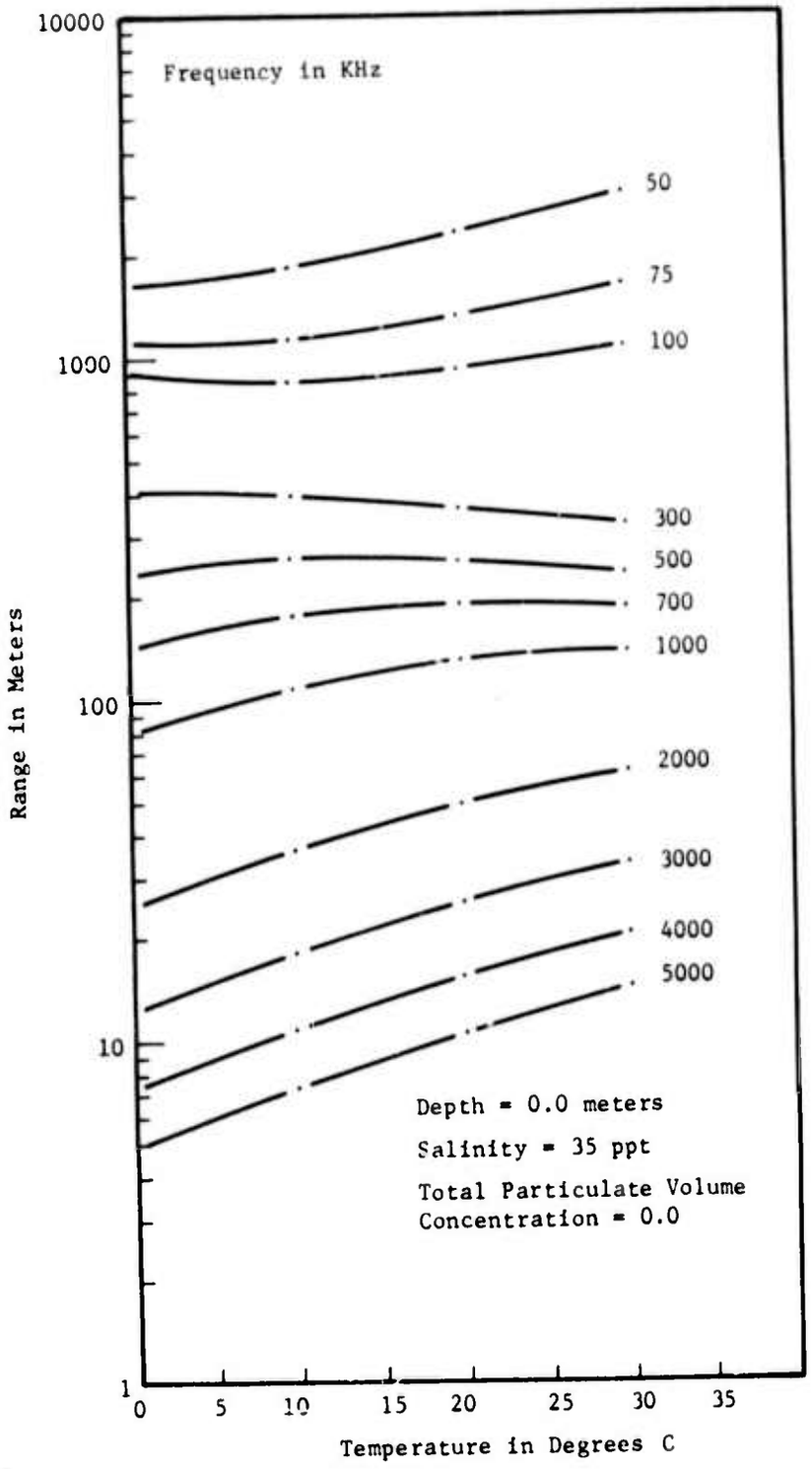

Figure 10a: Dependence of range as a function of temperature with frequency as a parameter.

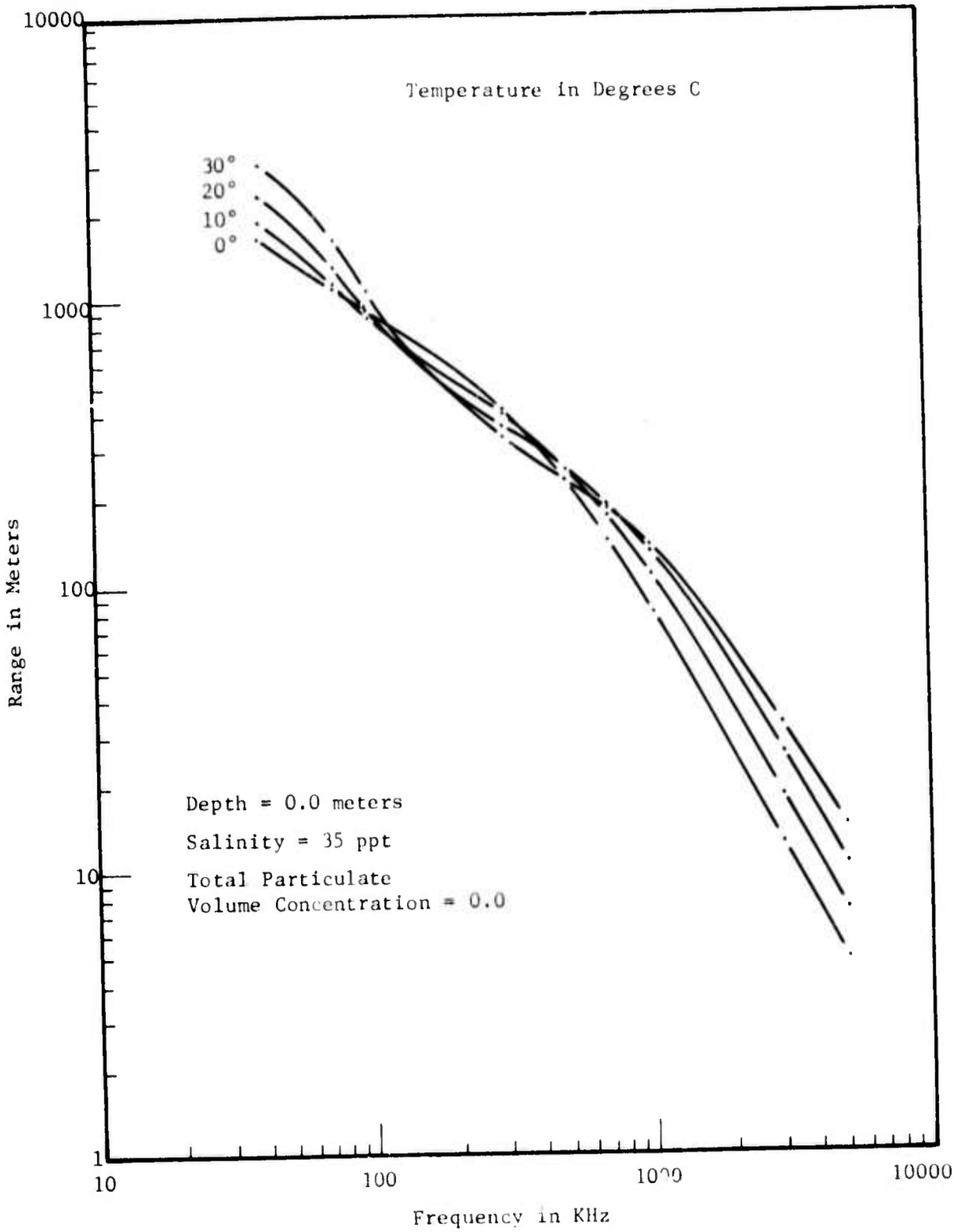

Figure 10b: Dependence of range as a function of frequency with temperature as a parameter.

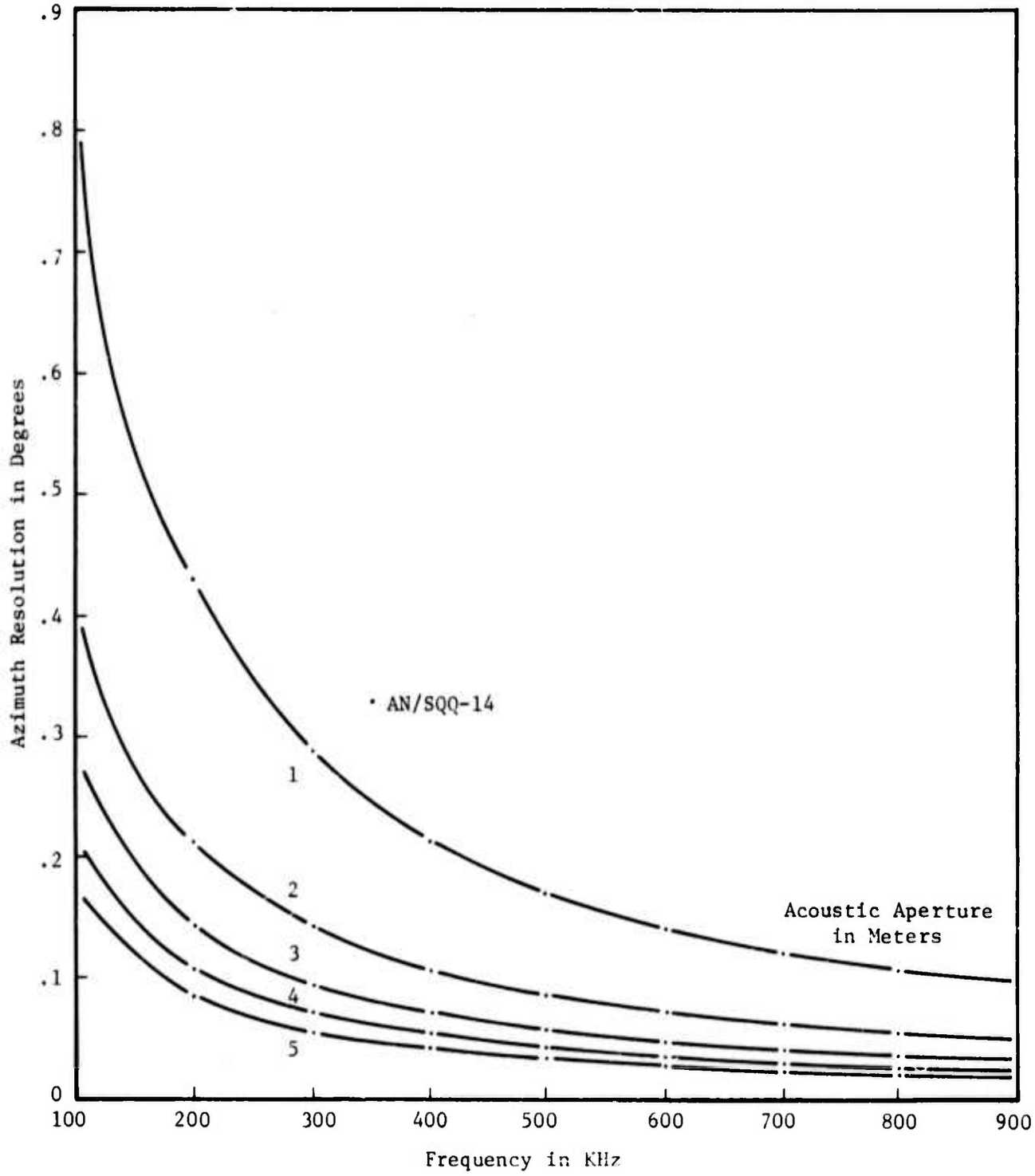

Figure 11: Azimuth resolutions as a function of frequency with acoustic aperture as a parameter.

4.0 LABORATORY EXPERIMENTS

Experimentation consisted of laboratory measurements verifying theory necessary for determining practical limitations on a low frequency acousto-optical imaging sonar. These experiments include measurements of the effect of acoustic reflectors on sensitivity (as reported in Section 3) and field of view.

4.1 Resolution

Under this phase of the contract, the resolution investigation was directed at resolving the disagreement between previously reported measurements (Ref. 1) and theory. This work included an observation that the wedge angle could be reduced with no resulting degradation in image resolution. This result suggests that the large cylindrical wedge formation lens is spherically aberrated. Thus, previous measurements could have been observed with a wedge angle smaller than the actual wedge angle used without a change in observed resolution. The result would then correspond more closely with theory. To quantitatively determine the effects of the cylindrical lens aberrations, the four foot acousto-optical imaging system configuration was employed. This configuration is referred to in Ref. 1 as the "improved" or "second" four foot acousto-optical imaging system. The only difference between the configuration used here and the configuration of Ref. 1 is an adjustable slit positioned between the diverging and collimating lens (see Figure 12). This slit can be adjusted to reduce the light wedge angle.

Resolution measurements consisted of observing two object transducers. The resulting two light spots in the image were then made to approach one another by moving the transducers together until the images were separated by the Rayleigh criterion. The distance between the two transducers was then measured and recorded as the acousto-optical imaging system resolution. Measurements were taken for a frequency of 500 KHz with the object transducers 15 feet from light/sound interaction region. As previously reported (Ref. 1), the resolution

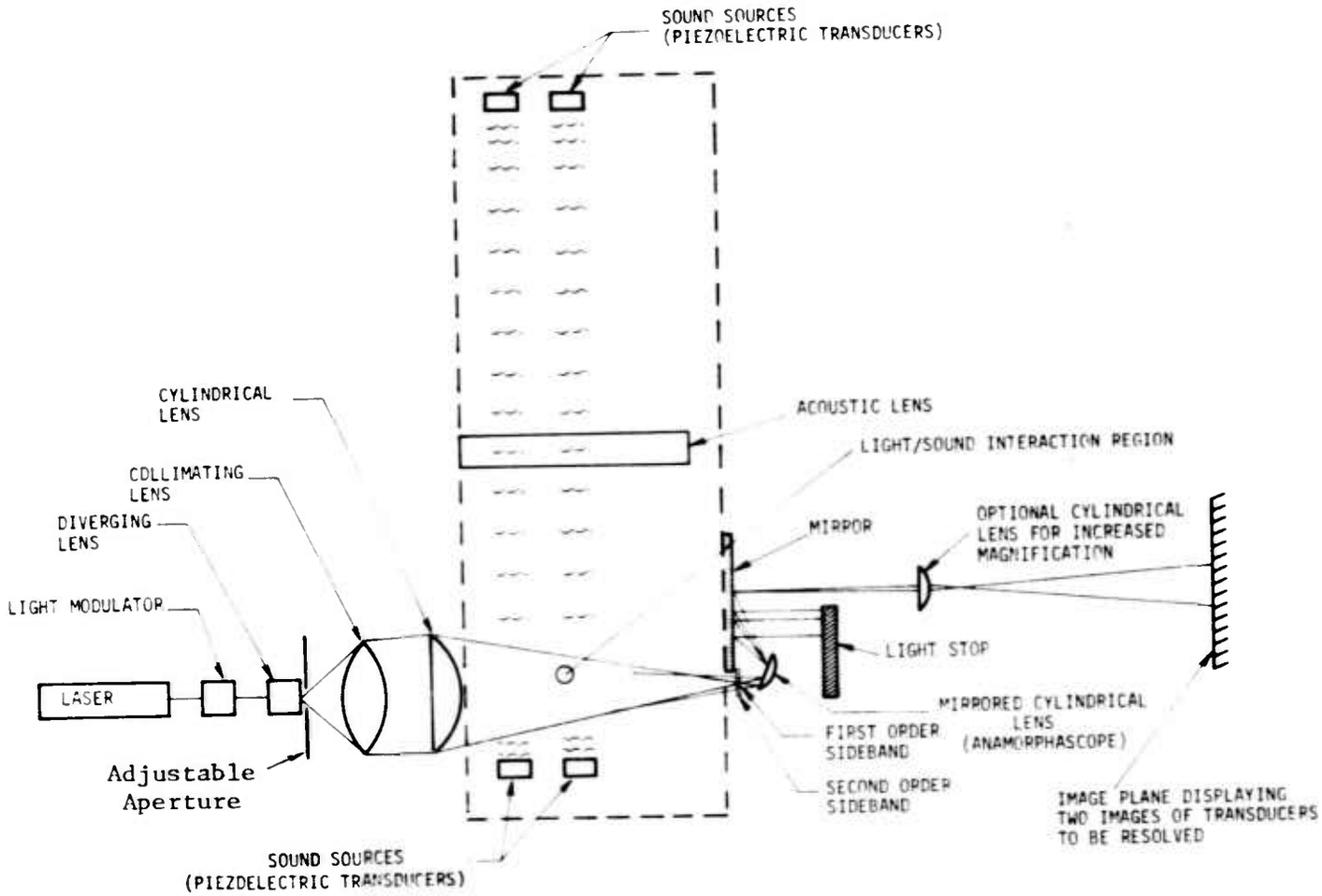

Figure 12: Second four-foot interaction cell acousto-optical imaging system.

was remeasured as 8.9 cm at 500 KHz. The slit positioned between the diverging and collimating lens was adjusted to reduce the light wedge angle. The light wedge angle was reduced until further reduction resulted in unresolved images. The minimum light wedge angle, α, where resolved images were observed, was measured and used in the theoretical expression for resolution. The computed theoretical valve was then compared with previous resolution measurements. The results are shown in Table 1.

Table 1: Comparison of Observed and Theoretical Resolution with Aberrated Light Removed

Frequency	Measured Resolution	Theory (New α) $\Lambda/2 \sin \alpha$
1.18 MHz	3.6 cm	4.1 cm
500 KHz	8.9 cm	9.6 cm
160 KHz	27.5 cm	30.0 cm
130 KHz	26.1 cm	36.9 cm

At all frequencies, measured resolution is better than predicted by theory. This can be explained with reference to Figure 13, containing a plot of image intensity for two mutually coherent point sources separated by the Rayleigh criterion.[10] If the two coherent sources are approximately 180° out of phase, the resolution will be better than predicted by theory. These results illustrate that a lens corrected for spherical aberrations could improve resolution by an order of magnitude with no change in lens size.

4.2 Resolution with a Parabolic Reflector

No resolution measurements for the vertical direction have previously been reported since these would depend more on acoustics than Bragg imaging.

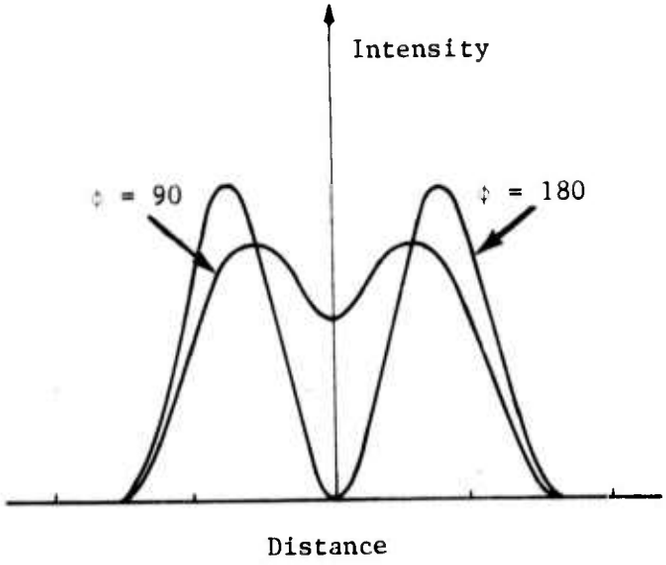

Figure 13: Intensity for two mutually coherent point sources separated by the Rayleigh criterion.

However, this is now a necessary part of the system. Therefore, vertical resolution measurements were taken with the acoustic lens used in Ref. 1 and with the parabolic acoustic reflector shown in Figure 14. The acoustic reflector was made parabolic in form by spinning casting resin at a constant rate until it solidified. The resulting contour was then coated with a flexible sheet of foam resin to provide a surface which is highly reflective to acoustic waves.

The object used to determine vertical resolution is shown in Figure 15. Two aluminum plates which can slide together were imaged by acoustic reflection. One plate was moved until the images satisfied the Rayleigh criteria. Typical images obtained using the acoustic lens and reflector are shown in Figure 16. Observed resolution using the acoustic reflector were found to be closer to theory than analogous data concerning the acoustic lens. Resolution characteristics observed with the acoustic reflector in place are presented in Table 2, along with similar results using the acoustic lens as reported in Ref. 1.

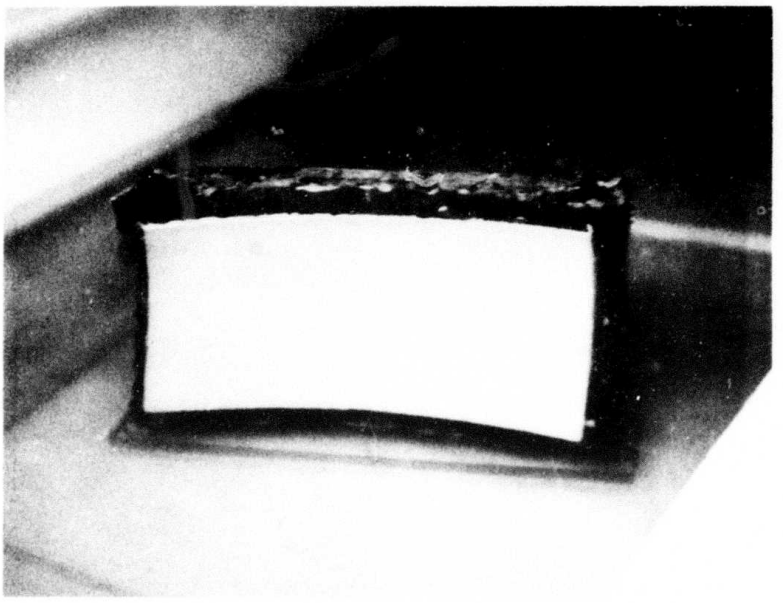

Figure 14: Parabolic acoustic reflector used for resolution measurements.

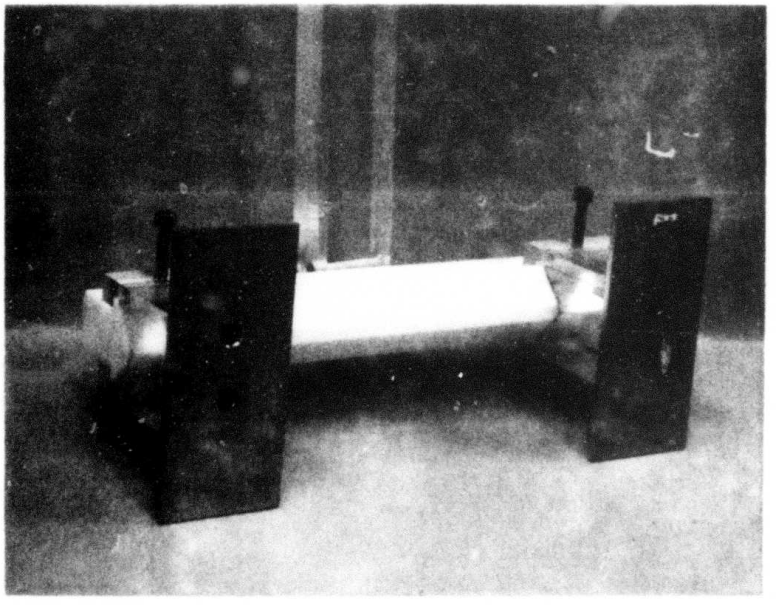

Figure 15: Object used for vertical resolution measurements.

(a)

Reflecting surfaces separated by 3.8 cm with the object 2 meters from the acoustic lens.

(b)

Reflecting surfaces separated by 1.9 cm with the object 2 meters from the acoustic reflector

(c)

Reflecting surfaces separated by 6.3 cm with the object 4.5 meters from the acoustic reflector

Figure 16: Images of two aluminum plates at 500 KHz used to determine the vertical resolution of the acousto-optical imaging system.

Table 2: Vertical Resolution Measurements Determining the Quality of an Acoustic Lens and Acoustic Reflector placed to Focus Sound into the Light/Sound Interaction Region.

Acoustic Processor	Frequency	Distance	Measured Resolution	ΔR/D
Lens	500 KHz	2 meters	3.8 cm	.8 cm
Reflector	500 KHz	2 meters	1.9 cm	1.1 cm
Reflector	500 KHz	4.5 meters	6.3 cm	2.5 cm

4.2.1 Field of View

As previously reported, the theoretical field of view (FOV) of the optical imaging system is limited to the acoustic aperture size when the image plane must not lie within central order light. Laboratory measurements confirm this situation. Although this is an excellent quality for short range research light sonars, larger fields of view are required for certain applications. A large FOV can be obtained with

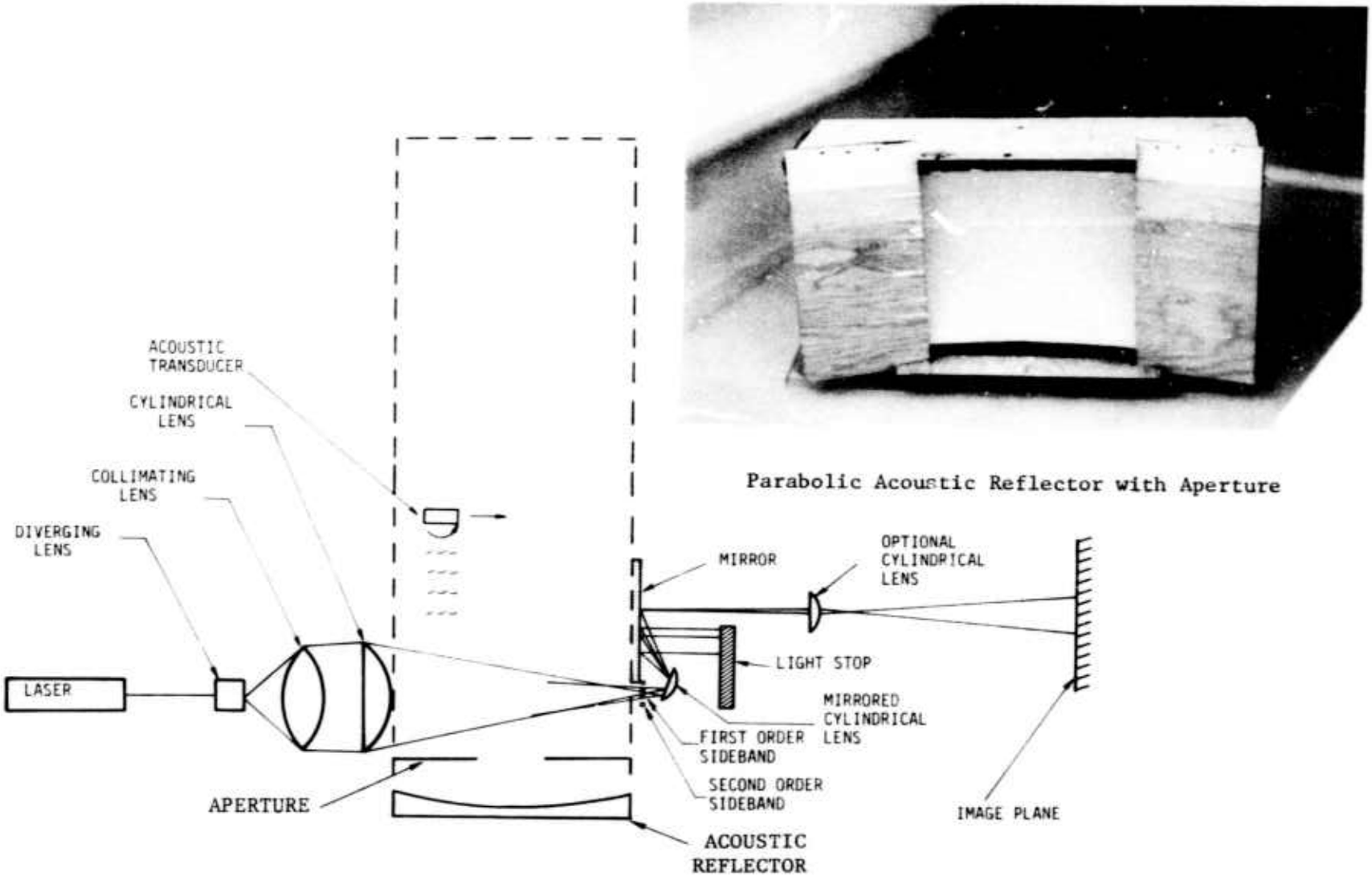

Figure 17: Four-foot interaction cell used for field of view measurement.

an acoustic reflector. A paraboloid reflector will concurrently increase the field of view in the horizontal direction and provide image focus in the vertical direction. To enable field of view experiments to be conducted in the facility, a reduction in acoustic aperture was made. This was accomplished by partially covering the parabolic acoustic reflector. The experimental configuration for the FOV experiment is shown in Figure 17. A transducer was traversed across the tank while position of a detector was adjusted for maximum signal return. In this manner, an azimuth field of view of 43° was measured. A field of view (FOV) as large as 100 degrees is quite feasible if the focal length of the acoustic reflector is made sufficiently short. This can be seen as easily feasible with reference to Figure 18. Figure 18 presents a ray trace for acoustic beams from distant objects near the limits of the FOV. The case shown in Figure 18 was contrived to show that the right angle condition for light diffraction can be satisfied in a system with a very large FOV by use of an acoustic reflector.

The system pictured in Figure 18 would use a paraboloid (Fig. 17) for two dimensional focusing. Note from the top view in Figure 18 that the full aperture may not be useful in causing light diffraction. Consider the plane pictured in the top view to illustrate the azimuth direction. Because the profile view is nearly at right angles everywhere, limitations introduced by the right angle condition place little constraint on the appearance of active sound rays shown in the profile view. This shows that it should be easier to obtain a large FOV in only one direction (elevation in Figure 18) than in both. A large FOV in elevation could be obtained with a cylindrical acoustic reflector.

4.3 Range Azimuth Imaging

A major difference in the operating modes of the system used in all previous experiments and that for a range azimuth imaging system is in orientation of the object plane which becomes the image plane. The object plane which is imaged by the range azimuth system is that

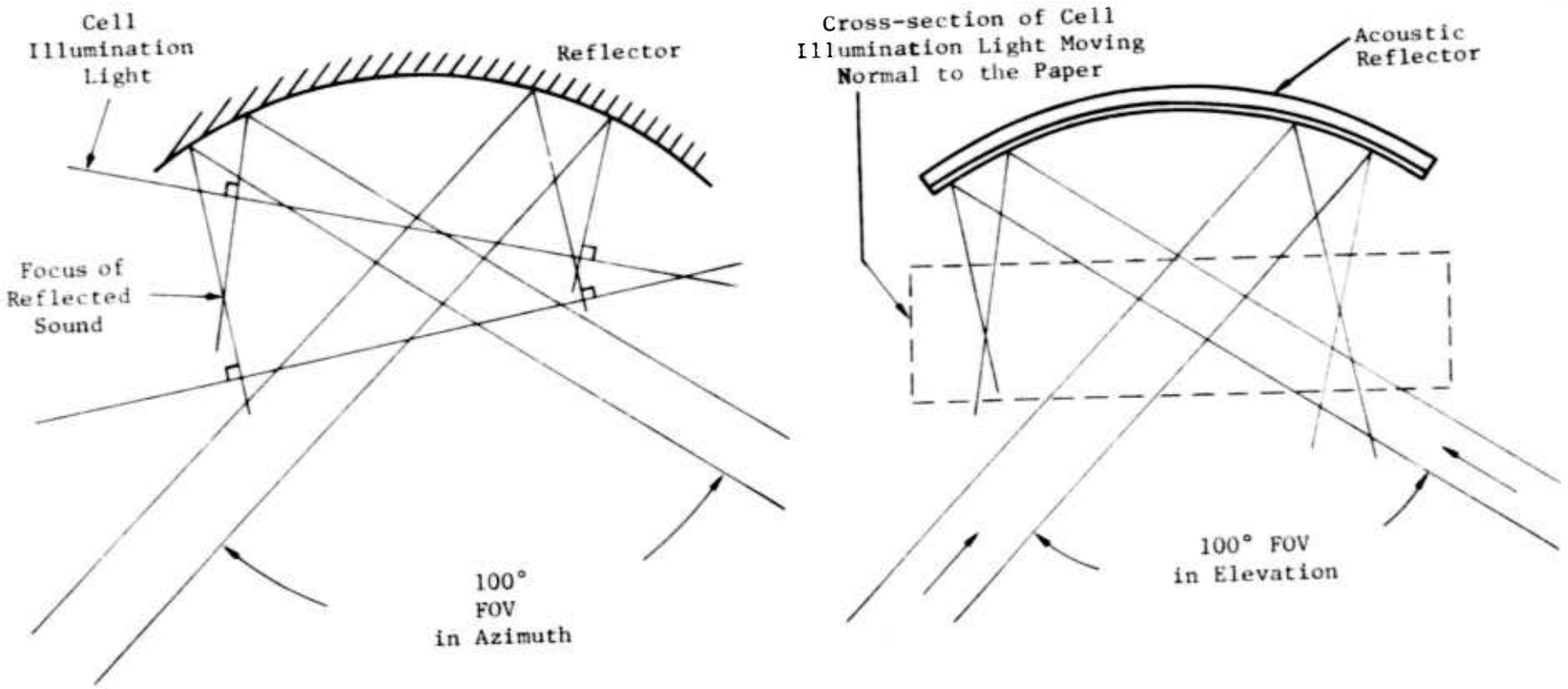

Figure 18 : Ray trace geometry for three-dimensional acoustic reflector behind light column.

the plane imaged is in the range-azimuth (or range-elevation) directions rather than a two-dimensional cross-range plane. That is, the detail shape found in a single cross-range direction is combined with detail found in range in order to get a two-dimensional image. In the system already described, the image was formed in two directions orthogonal to range. This system is illustrated in Figure 19. The characteristic which suggests that the image be formed in only one cross-range direction is simply that a large aperture is possible in only one direction. Attainment of detail found in range depends solely on the use of pulsed sound and the time required for sound to travel to the object and return. Resolution in the range direction is determined by duration of a pulse of sound. Cross-range resolution will be determined by the size of the aperture when the object viewed is in the far field. When the object viewed is nearby, the resolution is determined by the convergence angle describing cell illumination light.

To test the principle of range-azimuth imaging, the acousto-optical system was modified to generate range-azimuth images. Pulsed sound and light was used as illustrated in Figure 19. No acoustic lens or reflector is required and none was used for imaging. In this experiment, only image detail in azimuth is reproduced on the image plane. Image detail in elevation was suppressed by simply sensing variation in azimuth. Time of arrival of sound from the object which is imaged was converted to image detail in the other direction by a linear sweep in the vertical direction which was generated within the memory scope. Each horizontal position on the image plane was made to correspond to a horizontal position of a vertical line on the memory scope. The actual display generated on the scope corresponded to the time when sound from the object caused the writing action on the scope face in any given vertical line. One outgoing sound pulse was associated with one vertical sweep in the memory scope. The actual range interval which was recorded was determined by the delay provided between the sound pulse and occurrence of the light pulse due to diffraction within the Bragg cell. A complete

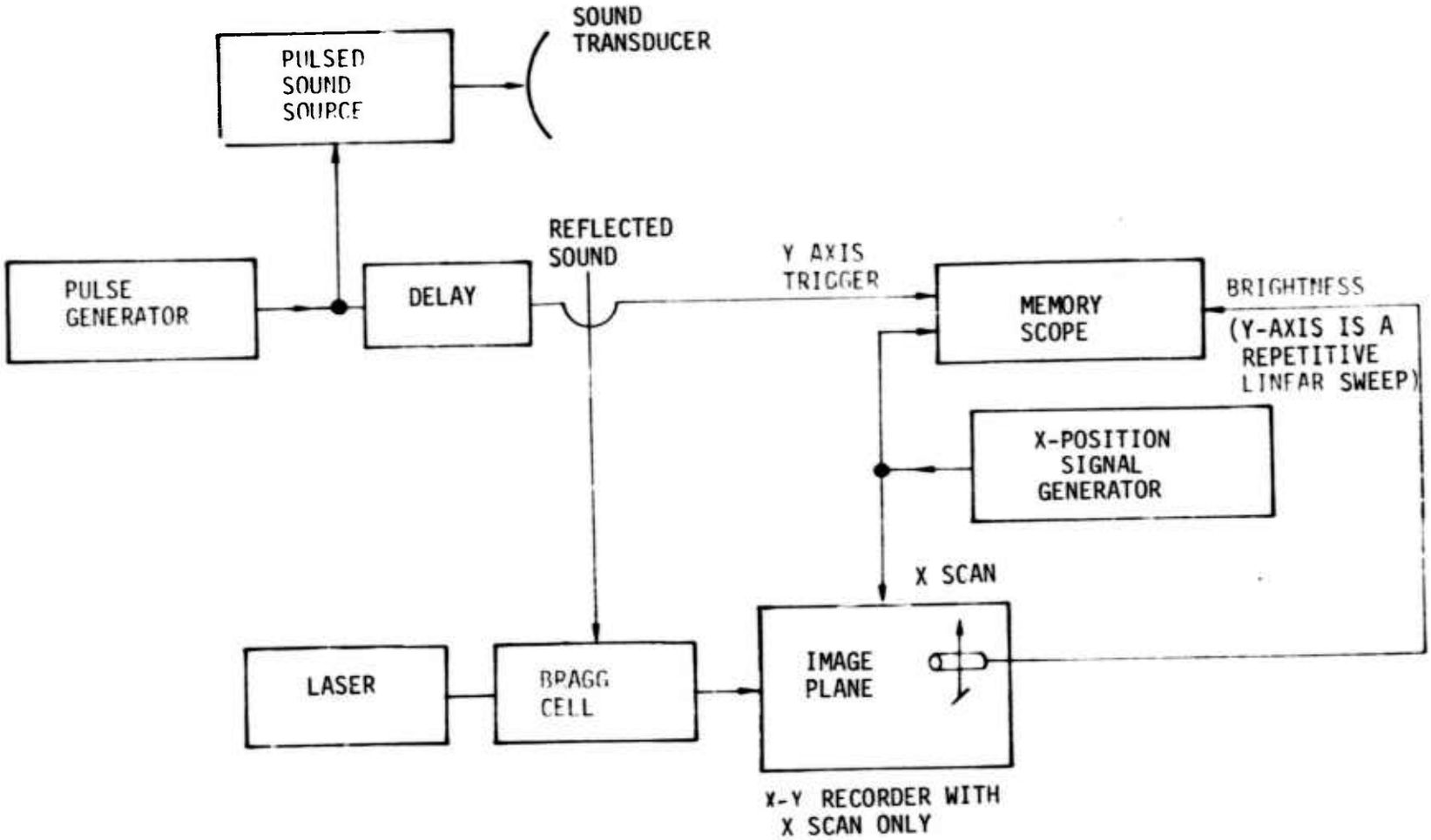

Figure 19: Block diagram of the range-azimuth imaging system.

image was formed by successively recording vertical lines continuously displayed horizontally until the entire horizontal width forming the image was scanned. The image shown in Figure 20 was made with this system using 500 KHz sound and a sound pulse width of 35 microseconds.

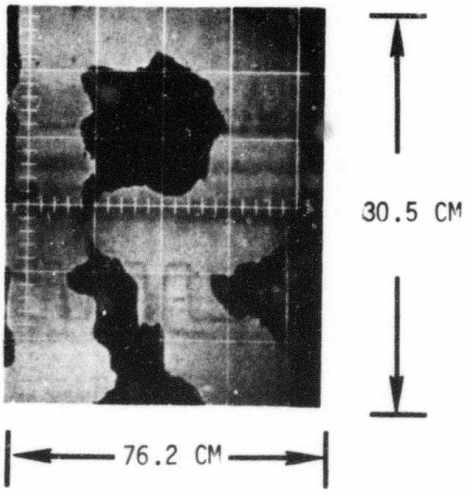

Figure 20: Range-azimuth image generated by tracing a 1-inch diameter sound transducer through a path in the form of the letter "R" and storing images formed by each successive position.

4.4 Improvement of Image Quality

Temperature gradients within water in the light/sound interaction have been observed to seriously degrade image quality. When the interaction region is quite long, even small gradients in water temperature will produce a gradient in the refractive index of the water and consequently, undesirable refraction of illumination light. As a result, an otherwise perfectly formed line of focus is distorted. The effect appears as a deviation from the straight line expected for the line of focus. A sideband image is similarly degraded. That is, a bend in the line of focus is replicated in the sideband image. This produces a regular distortion of the sideband image. This type of distortion will disappear when the line of focus is perfectly formed.

There are two basic approaches to preventing distortion of the line of focus. Mixing by keeping water in constant motion has proven to be quite effective in minimizing this type of distortion. Experiments reported here were performed to determine optimum flow rate in a typical imaging system which is four feet in interaction length. The second approach is based upon the observation that the refractive index of water is independent of temperature at 4°C. Small temperature gradients can therefore be allowed in water at 4°C, since there will be no associated refraction when the water is at 4°C.

4.4.1 Turbulent Mixing in the Light/Sound Interaction Region

To minimize the effects of temperature gradients, the experimental apparatus of Figure 21 was employed to turbulently mix the water of the light/sound interaction region. A flow diagram for this system is shown in Figure 22. By adjusting the inlet values of the tank, Figure 22,

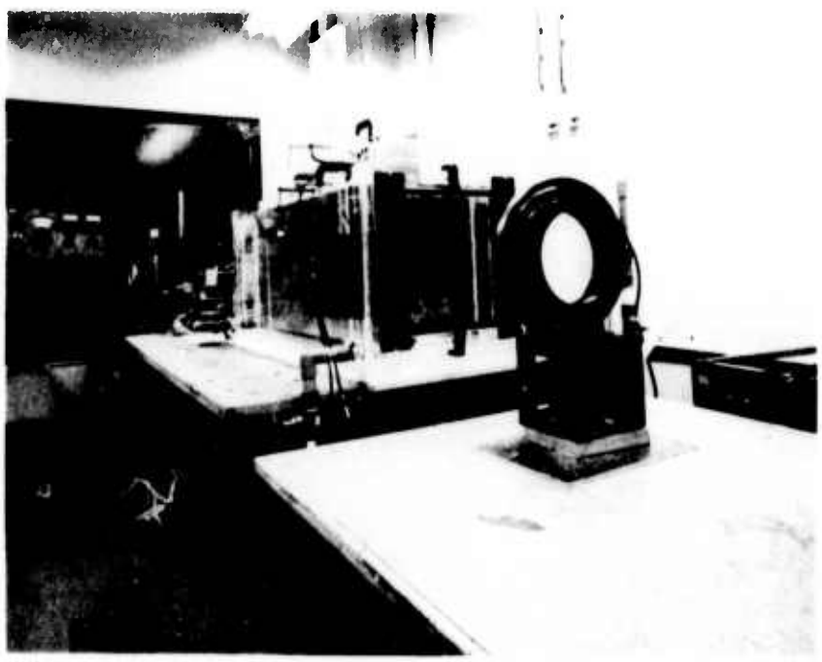

Figure 21: Acousto-optical imaging test configuration used for region cooling and mixing experiments.

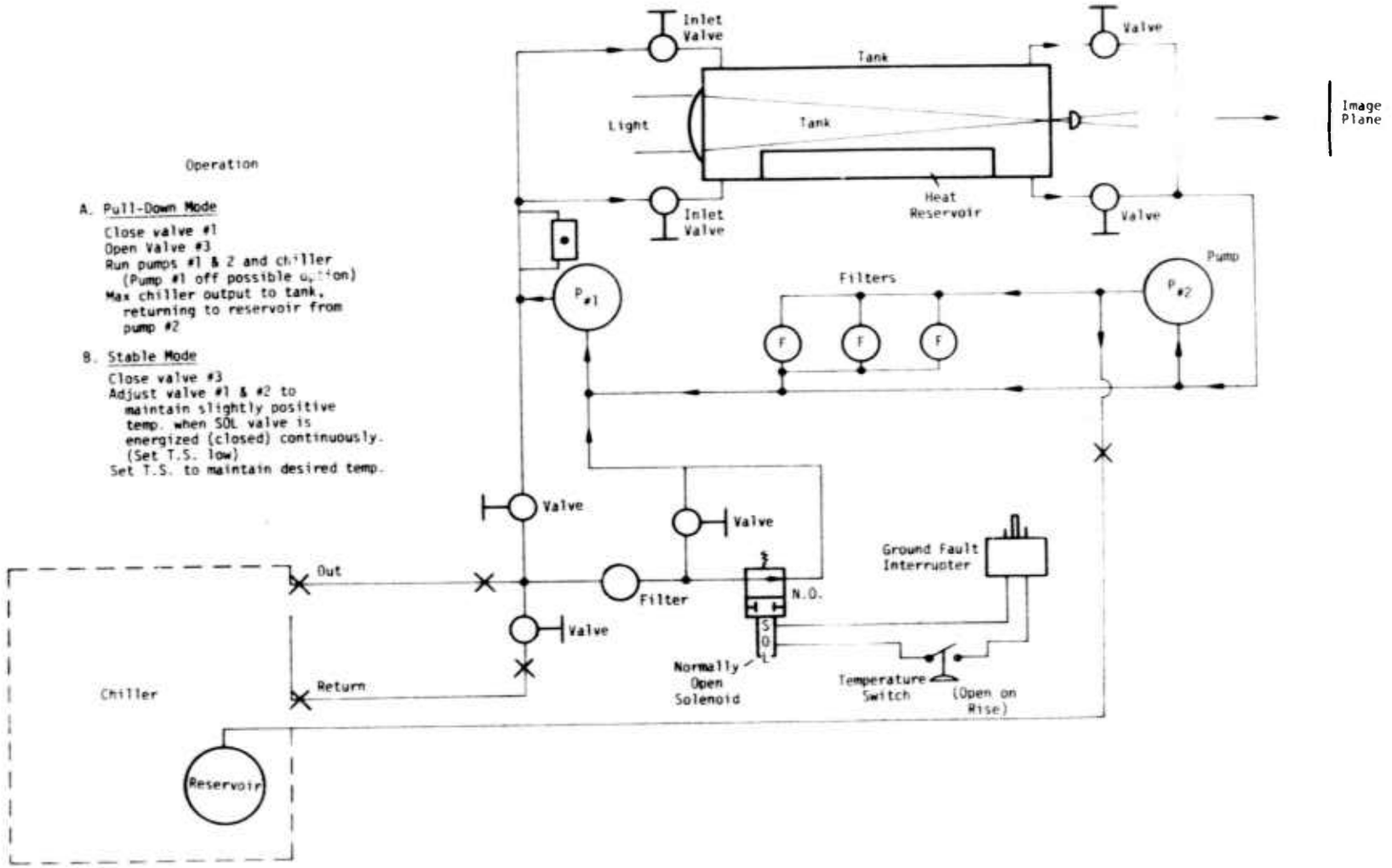

Figure 22: Light/sound interaction region cooling and mixing system.

various flow rates could be achieved. A sound transducer operating at 130 KHz was used to form images on each side of the central order light. The central order light and sideband images for flow rates of 6 and 12 gallons per minute (chiller off) are shown in Figures 23a and b, respectively. The images were then focused to a horizontal line which was scanned by a photodiode. The relative intensity, as a function of position for flow rates of 6 and 12 gallons per minute, is plotted in Figures 24a and b, respectively. The plot of relative intensity at 12 gallons per minute has better separation between the sideband and central order images than the plot at 6 gallons per minute. Both Figures 23 and 24 indicate that the higher flow rate of 12 gallons per minute improves image quality over the 6 gallons per minute rate.

4.4.2 Cooling of the Light/Sound Interaction Region to 4°C

The light/sound interaction cell of Figure 21 was used to demonstrate that image distortion due to temperature gradients could be reduced by maintaining the temperature of the cell at 4°C. The system was set up with the same lens and interaction length as used in the four foot system used in all previous imaging experiments described on previous pages. Equipment used to drive acoustic transducers and to scan a photodiode is shown on the left of Figure 21. The cooling system for the tank is shown in Figure 22. After the temperature of the tank was allowed to stabilize, the heat reservoir shown in Figure 22 was filled with water at 17°C. The temperature difference between the heat reservoir and the tank created a temperature gradient in the light/sound interaction region. Reference to Figure 25 shows that the effects of the temperature gradients are minimized at 4°C. The central order light shown in the photograph in Figure 23 was taken with a cell temperature of 4.0°C and 7.0°C, while the heat reservoir was maintained at 17.0° and 16.7°C, respectively.

4.5 Dual Frequency Heterodyning

Sensitivity calculated in Section 2.2 for a heterodyning system can be obtained in an imaging system by placing a square array of

a. Six gallons per minute flow rate

b. Twelve gallons per minute flow rate

Figure 23: Central order light and sideband images for turbulent mixing of the light/sound interaction region with two mixing flow rates.

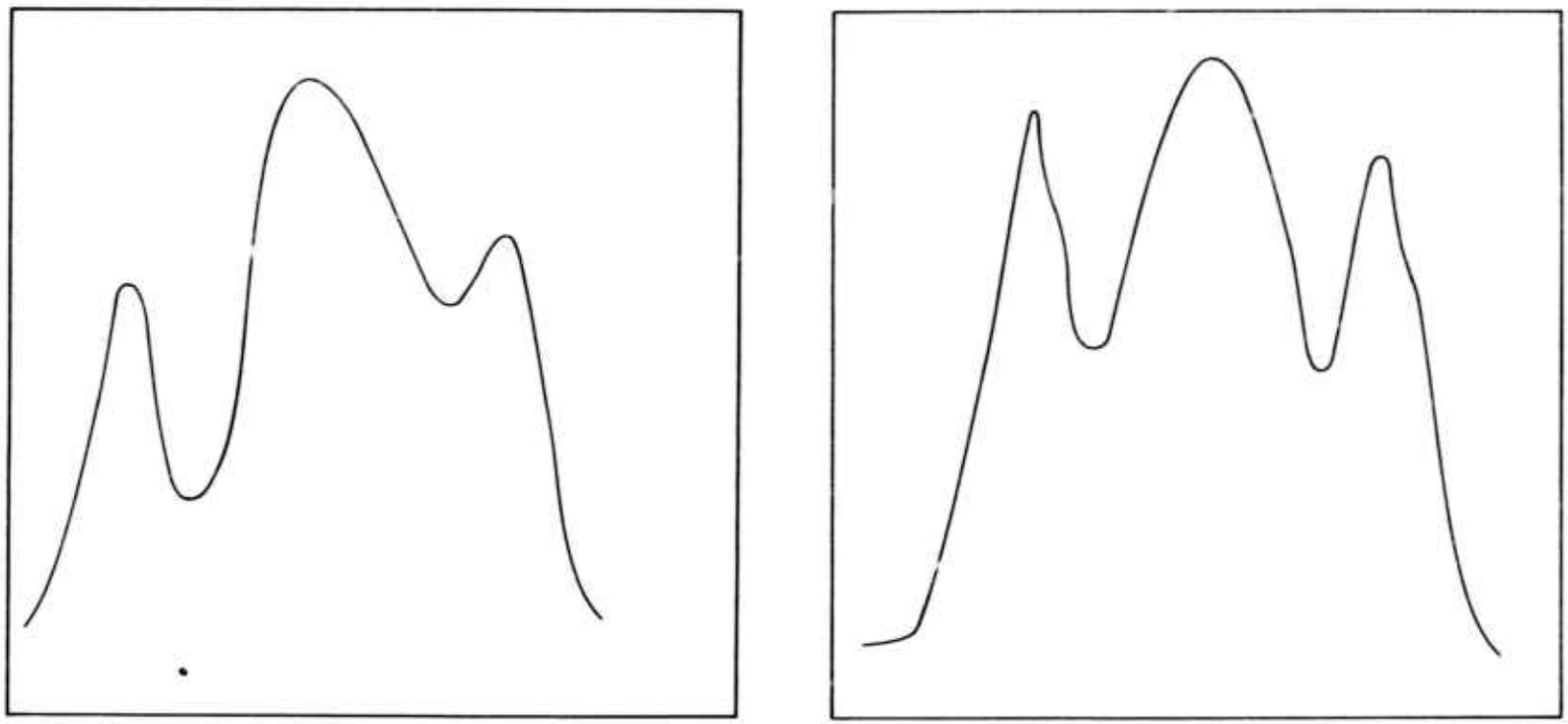

a. Six gallons per minute flow rate

b. Twelve gallons per minute flow rate

Figure 24: Relative intensity as a function of position for central order light and sideband images.

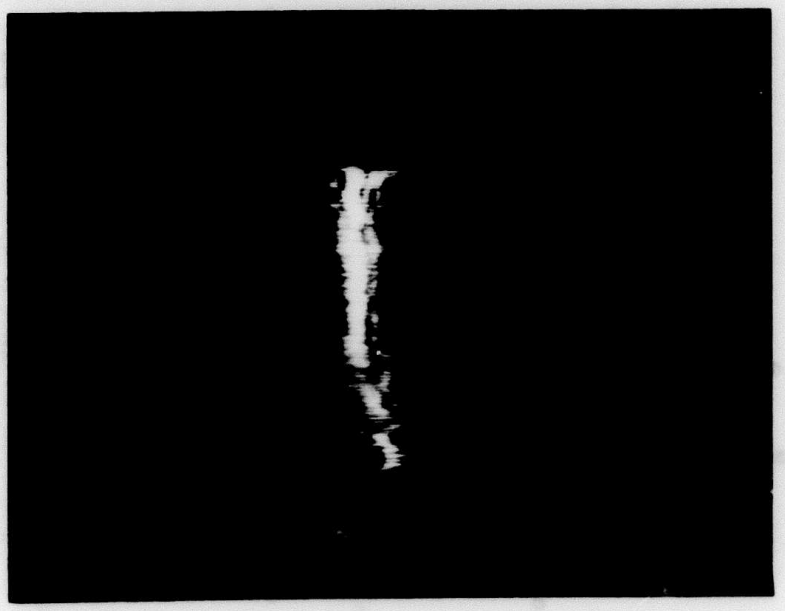

a. Tank temperature 4.0°C and heat reservoir temperature 17.0°C

b. Tank temperature 7.0°C and heat reservoir temperature 16.7°C

Figure 25: Images of central order light with temperature gradients in the light/sound interaction region.

photodiodes on the image plane. Each photodiode would then drive a narrow band amplifier and the output of each amplifier would drive an element in a display. To simulate this system at minimum cost, a single photodiode was scanned slowly over the image plane as illustrated in Figure 26. An x-y recorder was used as a transport for the photodiode and signals positioning the photodiode were used to position the spot position on a memory scope. Output from the photodiode was amplified in a lock-in amplifier and subsequently fed to the scope input controlling spot brightness (z-axis). Previously published experimental results concerning image formation in a heterodyne image pick-up system were results obtained with active acoustic projectors acting as the object to be viewed. This was done to simplify the task of estimating the acoustic level of the signal forming the image. The purpose of this section is to present an image formed by sound reflected from an object using the dual frequency heterodyne system described in Reference 1. The image obtained with this system is shown in Figure 27 together with the object reflecting sound forming the acoustic image. The sound level was sufficiently weak to render the image (on the image plane), too weak to be visible by direct viewing.

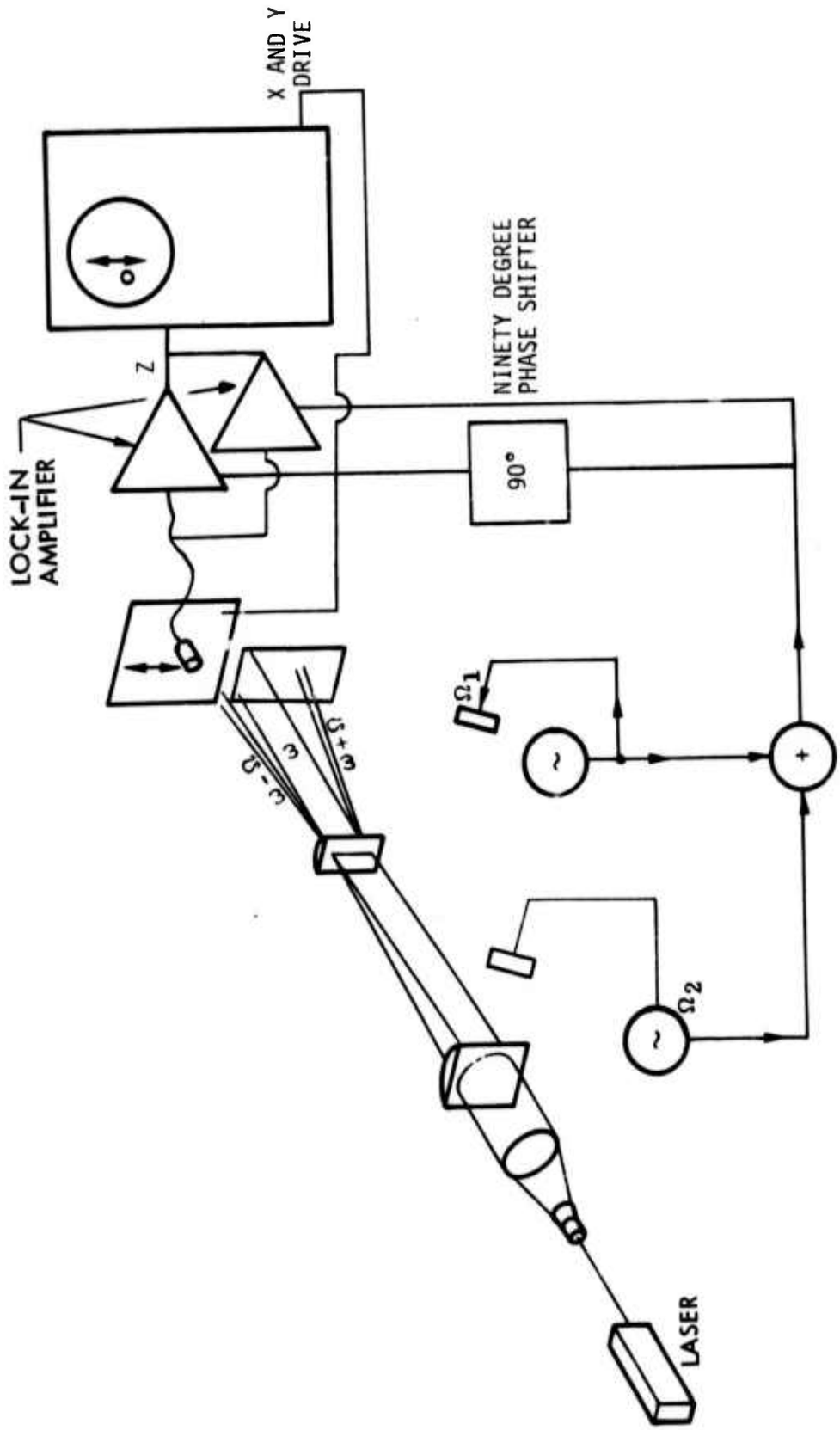

Figure 26: A dual frequency light-heterodyne acousto-optical system.

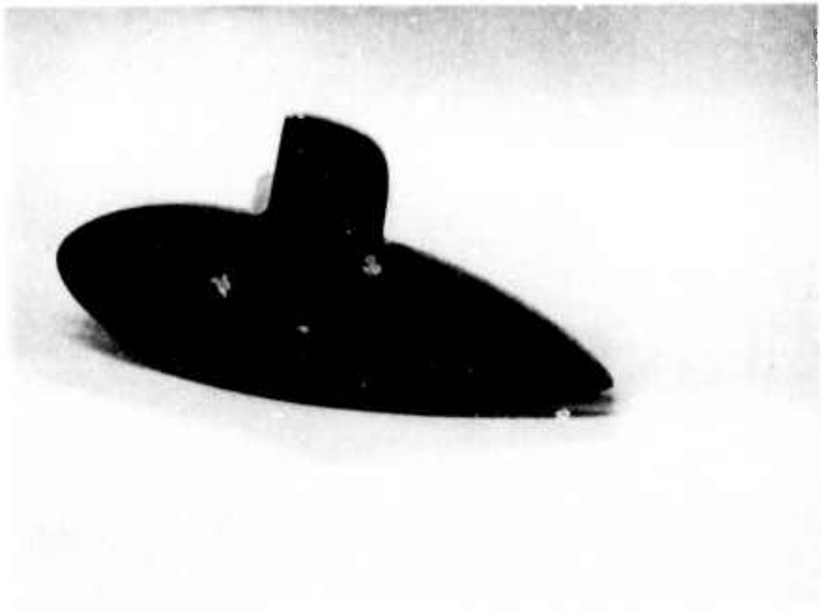

a. Object used for heterodyne imaging

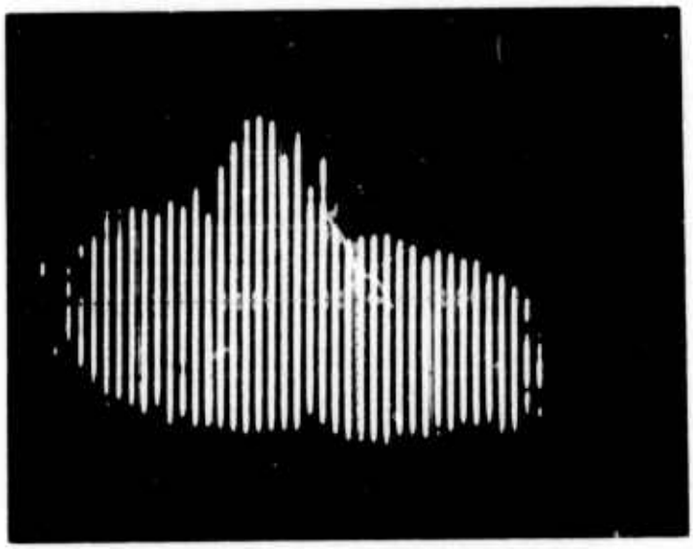

b. Heterodyned image of object 27a at 1.8 MHz

Figure 27: Dual frequency heterodyned reflection image at 1.8 MHz at a distance of 15 feet.

5.0 CONCLUSIONS

Operating range and resolution change with frequency were shown to be comparable with existing sonars. Measurement of sensitivity using a calibrated transducer showed that the acousto-optic system is more sensitive than previously reported[1] by 34 db. This provided the basis for projection of a new range capability. Additionally, projection of system resolution and range that should be ultimately attainable based on theory are shown in Figures 11 and 5, respectively. Almost any field of view can be constructed by bringing several similar elementary systems together into an integrated system. However, a field of view of 90 degrees is easily feasible in a single system which uses an acoustic reflector such as the unit constructed for this project (Figure 14).

Two techniques for improving image quality were tried and found successful. One of these consisted of cooling the light/sound interaction region down to 4°C. This operating temperature corresponds to the environmental temperature expected at great depths.

The mission profile for the acousto-optical imaging system, such as operating depth, viewing constraints and desired operating characteristics, has not yet been defined. As a result, it is too early to specify the housing for the laser beam and materials to be used. However, no difficulty is expected since the possible variation is so great. A primary problem area is the membrane which is required to separate the sea from the particle free water required in the light/sound interaction region. This can be solved by using a sheet of Tan-Rho-C rubber (B.F. Goodrich Co.) which has been formulated to match the acoustical impedance of sea water with negligible transmission loss.

6.0 REFERENCES

1. Smith, R. A., J. H. Cole, R. L. Johnson and P. G. Bhuta, "Feasibility Demonstration of Low Frequency Acousto-Optical Imaging for Sonar Applications," TRW Systems report 8520.2.73-110, 12 July 1973.
2. "High Resolution Sonar Technology (U)," Vol. I - Summary, Conclusions, and Recommendations in Relation to Operational Navy Requirements (U), Control No. 69-R-1112, January 1969, Confidential; Vol. II, A Collection of Background Papers (U), Control No. 69-R-1367, March 1969, Confidential. Prepared by High Resolution Sonar Study Panel of the Mine Advisory Committee.
3. Korpel, A., "Visualization of the Cross-Section of a Sound Beam for Bragg Diffraction of Light," Appl. Phys. Letters, 9:425-427 (15 December 1966).
4. Wade, G., C. J. Landry and A. A. deSouza, "Acoustic Transparencies for Optical Imaging and Ultrasonic Diffraction," presented at the First International Symposium on Acoustical Holography, Huntington Beach, Calif., 1967 [Subsequently published in Acoustical Holography, edited by A. F. Metherell, H.M.A. El-Sum, and Lewis Larmore (Plenum Press, Inc., New York, 1969), Vol. I].
5. Korpel, A., "Acoustic Imaging by Diffracted Light. I. Two-Dimensional Interaction," IEEE Trans. on Sonics and Ultrasonics, SU-15(3): 153-157 (July 1968).
6. Aprahamian, R., J. L. Jacoby and P. G. Bhuta, "Nondestructive Testing Using TRW Acousto-Optical Imaging System," Army Materials and Mechanics Research Center Report AMMRC CR 71-4/2, August 1971.
7. Aprahamian, R. and P. G. Bhuta, "Acousto-Holographic Method and Apparatus for Internally Imaging and Interferometrically Analyzing Objects," U.S. Patent No. 3,626,753, filed March, 1970.
8. Winter, D. C., "Noise Reduction in Acousto-Optic (Bragg) Imaging Systems by Holographic Recording," Appl. Phys. Letters, 15 Feb. 1973.
9. Smith, R. A. and G. Wade, "Noise Characteristics of Bragg Imaging," Chapter 6 in Acoustical Holography, Vol. 3, A. F. Metherell Editor, Plenum Press, 1971.
10. Goodman, J. W., Introduction to Fourier Optics, McGraw-Hill, 1968, pgs. 86 and 87.
11. Smith, R. A., et al., Reference 1, page 11.
12. Sears, F. W., Optics, Addison-Wesley Press, 1949, page 221.
13. Brillouin, L., "Diffusion de la lumiere et des rayons x par un corps transparent homogene," Amm. Phys. (Paris) 9th Ser. 17:88 (1922).
14. Urick, R. J., Principles of Underwater Sound for Engineers, McGraw-Hill Book Co., page 167, 1967.

15. Smith R. A., "Noise Limitations on Ultrasonic Imaging, Ph.D. Dissertation, University of California, Santa Barbara (March 1971).

16. Bhatia A. B. and W. J. Noble, "Diffraction of Light by Ultrasonic Waves: I. General Theory and II. Approximate Expression for the Intensities and Comparison with Experiment," Proc. Royal Soc., Vol. A220, pp. 356-385, 1953.

17. Raman, C. V. and N. S. Nagendra Nath, Proc. Indian Acad. Sci., Vol. 2, 413 (1935).

18. C.f., Carlson, Bruce A., Communication Systems, McGraw-Hill Book Co., New York, 1968, p. 279.

19. Yariv, A., Quantum Electronics, Wiley Book Co., 1967, p. 453.

20. Urick, R. J., Principles of Underwater Sound for Engineers, McGraw-Hill Book Co., page 20, 1967.

21. McLeroy, E. G., "A Brief Analysis of the Effect of Solid Particles on Sonar Performance," U.S. Navy Mine Defense Lab., Panama City, Florida Report i-100 (March 1966).

22. Smith, R. A., et al., "Studies of Resolution in a Bragg Imaging System," J. Acoust. Soc. Am. 40, pp 1062-1068, March 1971.

23. Pratt, W. K., Laser Communication Systems, John Wiley and Sons, Inc. N.Y., 1969.